Stability of Triple-Helical Poly(dT)-Poly(dA)-Poly(dT) DNA with Counterions

Voichita M. Dadarlat and V. K. Saxena
Department of Physics, Purdue University, West Lafayette, Indiana 47907 USA

ABSTRACT Structural conformation of triple-helical poly(dT)-poly(dA)-poly(dT) has been a very controversial issue recently. Earlier investigations, based on fiber diffraction data and molecular modeling, indicated an A-form conformation with C_3'-*endo* sugar pucker. On the other hand, Raman, solution infrared spectral, and NMR studies show a B-form structure with C_2'-*endo* sugars. In accordance with these experimental results, a theoretical model with B-form, C_2'-*endo* sugars was proposed in 1993. In the present work we investigate the dynamics and stability of the two conformations within the effective local field approach applied to the normal mode calculations for the system. The presence of counterions was explicitly taken into account. Stable equilibrium positions for the counterions were calculated by analyzing the normal mode dynamics and free energy of the system. The breathing modes of the triple helix are shifted to higher frequencies over those of the double helix by 4–16 cm^{-1}. The characteristic marker band for the B conformation at 835 cm^{-1} is split up into two marker bands at 830 and 835 cm^{-1}. A detailed comparison of the normal modes and the free energies indicates that the B-form structure, with C_2'-*endo* sugar pucker, is more stable than the A-form structure. The normal modes and the corresponding dipole moments are found to be in close agreement with recent spectroscopic findings.

INTRODUCTION

The biological processes of metabolism and replication in the cells of living organisms can be partly explained in terms of the basic units of the deoxyribonucleic acid (DNA) molecules. The DNA molecule accomplishes these functions through its double-helical structure. In 1957, Felsenfeld and co-workers discovered triple-helical DNA and pointed out that the three-stranded structure "may have significance as a prototype for a biologically important three-stranded complex as, for example, a single ribonucleic acid chain wrapped around two stranded DNA." It was not until the last decade that significant research interest in this specific type of DNA was revived, because of the realization that the triplex offered a very strong potential in biological and pharmacological applications.

The triplex DNA molecule is a triple-helical polymer, each strand of which is composed of nucleotides held together sequentially by means of sugar-phosphate connections. This assembly is referred to as the backbone. Hydrogen bonds link complementary bases on the three strands, i.e. adenine to thymine or guanine to cytosine, forming the so-called triplets. Triplex formation (Saenger, 1984) involves the binding of an oligonucleotide strand (strand III) to the major groove of a Watson-Crick base-paired (strands I and II) duplex of DNA, thus forming Hoogsteen or reversed Hoogsteen hydrogen bonds with the polypurine strand of the pyrimidine-purine duplex.

The new structure has three grooves that are named in relation to the bonding scheme between the strands that define each groove (White and Powell, 1995). The groove between the I and II strands is called the Watson-Crick groove, and it is similar to the minor groove in the double helix. The groove between strands II (purine) and III (second pyrimidine) is called the Crick-Hoogsteen groove. The third groove is between the first and third strands and is called the Watson-Hoogsteen groove. The Crick-Hoogsteen and the Watson-Hoogsteen grooves share the initial major groove of the double helix.

The first observation of the formation of the triple helix (Felsenfeld et al., 1957) was in the synthetic $r(U)_n$-$r(A)_n$-$r(U)_n$ in the presence of Mg^{2+}. Since then, other types of triple helices have been synthesized, and biological mechanisms involving the triple helices have been proposed (Hsieh and Camerini-Otero, 1990; Zhurkin et al., 1994; Kim et al., 1995). Despite the interest and intense activity on triple helices, there is very little precise structural information available for these complex systems. Arnott and coworkers (Arnott and Selsing, 1974) used molecular modeling and fiber diffraction data to give the first detailed DNA triple helical structure for $d(T)_n$-$d(A)_n$-$d(T)_n$ in 1974, and they concluded that the structure is A-form DNA and has a C_3'-*endo* sugar pucker. For many years this model has been the structural basis for work on DNA triple helices.

In 1983, G. A. Thomas and W. L. Peticolas, using Raman spectroscopy studies, showed that the DNA triple helix adopts a B conformation, C_2'-*endo* sugars, in solution.

Recent solution infrared spectral studies (Howard et al., 1992) and NMR studies (Macaya et al., 1992) also indicate that the polynucleotide helix $d(T)_n$-$d(A)_n$-$d(T)_n$ has a B-form structure and sugar puckers in the C_2'-*endo* region. In

Received for publication 18 August 1997 and in final form 31 March 1998.

Address reprint requests to Dr. V. K. Saxena, Department of Physics, Purdue University, 1396 Physics Building, West Lafayette, IN 47907-1396. Tel.: 317-494-9575; Fax: 317-494-0706; E-mail: saxena@physics.purdue.edu.

Dr. Dadarlat's present address is Department of Medicinal Chemistry and Molecular Pharmacology, Purdue University, West Lafayette, IN 47907.

0006-3495/98/07/70/22 $2.00

1993, Raghunathan, Miles, and Sasisekharan proposed a new model for the triple helix in accord with these experimental findings. In this new model the three strands of the triple helix are related by symmetry, so that the backbone conformations are all the same.

Long tracts of dA_n-dT_n (the so-called A-tract DNA) in double-helical DNA were made accountable for the DNA bending adjacent to these specific stretches of DNA (Chan et al., 1990). The A-T-rich double-helical DNA adopts a secondary structure that is slightly different (Erfurth et al., 1972) from the standard B-DNA structure, the so-called B′-DNA. By analogy, our triple-helical $d(T)_n$-$d(A)_n$-$d(T)_n$ B form should be called the B′ form of $d(T)_n$-$d(A)_n$-$d(T)_n$. This further motivates the study of $d(T)_n$-$d(A)_n$-$d(T)_n$ triple-helical DNA.

The common features for the two available structures of $d(T)_n$-$d(A)_n$-$d(T)_n$ are the number of residues per turn (n = 12) and the axial rise per residue (h = 3.26 Å). The thymine1 strand is connected to the adenine strand via Watson-Crick-type hydrogen bonds, and the thymine2 strand is connected via Hoogsteen-type hydrogen bonds. The hydrogen bond lengths are listed in Table 1. In the A conformation the Hoogsteen-type hydrogen bonds are longer than the corresponding ones in the B conformation, which leads to a significant difference in the bonds' strength. In the A conformation the bases are tilted by 8.5° with respect to the helix axis, whereas in the B conformation they are almost perpendicular to the helix axis. As mentioned before, the only parameters determined experimentally are the number of residues per turn and the axial rise per residue.

The symmetry elements for each structure are the constraints imposed in the molecular modeling procedure. For the B conformation, a 2.5-Å displacement of the bases from the helix axis, a rotational angle of 180° around the x axis between the Watson-Crick paired adenine and thymine1 strands, and a rotational angle of 69.5° around the z axis between the Hoogsteen paired adenine and thymine2 strands were necessary to obtain a stereochemically satisfactory structure for the triple helix while maintaining symmetry among all three strands. All torsional angles are within allowed ranges for the type of structure they are in. The diameter of the helix is 22.24 Å for the A conformation and 24.4 Å for the B conformation. In our calculations we have used the coordinates of the atoms in the B conformation following the model proposed by Raghunathan and co-workers.

TABLE 1 Hydrogen bond lengths and strengths in triple-helical DNA

		S-type sugars		N-type sugars	
Bond type	H-Bond	r_{eq}	K	r_{eq}	K
Hoogsteen	N_6-O_4	2.7127	0.383	2.8984	0.061
	N_7-N_3	2.8720	0.154	2.9463	0.071
Watson-Crick	N_6-O_4	2.8881	0.079	3.0557	0.015
	N_1-N_3	2.9143	0.100	2.7997	0.304

Values are in millidynes/Å.

The high specificity of the binding of a third strand oligonucleotide to an associated duplex provides a powerful artificial endonuclease (Moser and Dervan, 1987; Strobel et al., 1991). It has been shown that this activity has strong applications in genome mapping (Strobel et al., 1991). The site-specific character of triplex formation holds strong promise for using these structures as therapeutic agents. The binding of the triplex-forming oligonucleotides in a gene promoter region has been shown to regulate the gene expression by blocking its transcription through the inhibition of mRNA synthesis (Duval-Valentin et al., 1992).

Any biological activity of double- or triple-helical DNA involves motions of atoms, groups of atoms, or distinct subunits of the macromolecule. These motions are strongly affected by the surrounding aqueous medium, the concentration of the solution, the ion concentration, and the type of positive ions. Infrared spectroscopy (Wittlin et al., 1986; Powell et al., 1987) and Raman spectroscopy (Thomas and Peticolas, 1983; Benevides and Thomas, 1983; Edwards and Liu, 1991) offer useful information about these motions. Recently, Fourier transform infrared (FTIR) spectroscopy has been used to investigate the midinfrared spectra of some samples of oligonucleotide triplexes (White and Powell, 1995).

Triplex-forming oligonucleotides (TFO) induce symmetry breaking and localized structural changes in the associated duplex structure. The vibrations involving the localized motions of a structural variation in a polymer are, in principle, fewer in number and well separated compared to the resonant propagating modes of an unchanged polymer (duplex DNA). The localized structural variations, due to triplex formation, produce their distinctive spectroscopic signatures. Spectroscopic observations of these signatures provide useful information about the binding energies of the third strand.

The stability of the triple DNA macromolecules is a central issue in the studies related to these systems (Cheng and Pettitt, 1992). Not any type of duplex will allow triplex formation. Strongly bent or very rigid duplexes are unlikely to form triplexes. Uniformity in the helical chain seems to be important for triplex formation. At a macroscopic level, the pH value of the solution, the hydration of the macromolecule, the ionic strength, and concentration of the positive ions in the solution all have a specific role in the stability of the macromolecule. To understand what factors are controlling triplex formation and its stability in vivo, where intracellular pH oscillates around 7.2, a neutral pH has to be maintained for the triplex solution.

The ultimate goal of the research activity in the DNA triple helices is to design oligonucleotides that will recognize any unique base sequence and form a stable triplex in the promoter region. An understanding of the microscopic parameters necessary for the stability of these structures is very important. For the genetic medication to become practical, the rules of the association and the interaction between

different units of the polymer, as well as the interaction of the triplex with the surrounding electrolyte containing water and counterions, should be precisely understood.

This paper explores the stability of triple-helical DNA polymers within the framework of solid-state physics. The first step of the calculations is to model the triplex as a very long, one-dimensional lattice and then to construct the force constant matrix and find its eigenvectors and eigenvalues. Analyzing the eigenvalues and eigenvectors, one can draw very useful conclusions about the normal modes of the system, its stability, and characteristics. Comparing the results with the experimentally found features, one can verify the validity of the model.

In the next section, the dynamical problem is set up in terms of equations of motion for the atoms in the unit cell of the lattice in the harmonic approximation. Various bonded and nonbonded interactions and the corresponding force constants for a monomer are defined. The third section includes the effect of counterions and the hydration sheath (including the bulk water) on the dynamics of the system. This is accomplished by the effective field approach (Saxena et al., 1989). The new equations of motion for the triplex DNA + hydration sheath + counterions + bulk water system are set up. The stability of the system is studied as a function of the counterion positions, the dielectric constant inside the triple DNA, and the weak covalent bonding between the counterions and the free oxygens in the phosphate groups. A calculation of the free energy, to support our normal mode analysis for the system, is also presented in this section.

The resulting normal modes and their relation to various atomic motions, including hydrogen-bond breathing and sugar-pucker modes, are presented in the fourth section. This section also contains a discussion of the consequences of various parameters for the stability of the triplex, along with a comparison with existing experimental data. Finally, the fifth section contains a discussion of our results and conclusions about the structure and relative stability of the two conformations of the triple-helical structures.

THE DYNAMICAL PROBLEM

Equations of motion in the harmonic approximation

To find the solution to the dynamic problem, we model the triple DNA molecule as a very long, one-dimensional lattice, with the axis of the helix parallel to the z axis and the xy plane perpendicular to it. The base triplets are stacked one after another at 3.26 Å along the z axis, with a relative rotation angle of $\psi = 30°$ between adjacent triplet bases (the symmetry elements are the translation along the z axis and rotation around the z axis). This lattice will have one triplet as a unit cell.

Each triplex DNA macromolecule has N unit cells and M atoms in each unit cell (M is actually 61 and N is on the order of hundreds of thousands). This system will have $3NM$ degrees of freedom. The atoms are arranged in a left- or right-handed triple-stranded helical symmetry. Let m_i be the mass of the ith atom ($i = 1, 2, \ldots, 3M$) and x_{in} be the Cartesian displacement of the ith atom in the unit cell n. $i = 1, 2, 3$ relates to atom 1 (x, y, or z components), $i = 4, 5, 6$ to atom 2, and so on.

Equations of motion for this system form a set of $3NM$ coupled differential equations given by

$$\ddot{q}_{in} + \frac{\partial V}{\partial q_{in}} = 0 \tag{1}$$

where $q_{in} = \sqrt{m_i}x_{in}$ are the mass weighted Cartesian displacement coordinates, and x_{in} is the Cartesian displacement for the corresponding atom coordinate. Expanding the potential energy function V in powers of q_{in}, the equations of motion, within the harmonic approximation (because here we are interested in the linear phonon spectrum), can be written as

$$\ddot{q}_{in} + \sum_{jn'} F_{ij}^{nn'} q_{jn'} = 0 \tag{2}$$

where the harmonic force constants are given by

$$F_{ij}^{nn'} \equiv \left(\frac{\partial^2 V}{\partial q_{in}\partial q_{jn'}}\right)_0 \tag{3}$$

Equation 2 forms a set of $3NM$ coupled second-order linear differential equations describing the molecule in a harmonic force field. Within the periodic boundary conditions,

$$q_{in} = \exp(in\theta)\cdot q_{i0} \tag{4}$$

We seek solutions of the type

$$q_{in} = C_i \cdot \exp(-iwt)\cdot \exp(in\theta) \tag{4}$$

where θ is the phase difference between the oscillations in the adjacent cells. The boundary condition determines the admissible values for θ. Appropriate substitutions lead us to

$$w^2 C_i = \sum_j \mathcal{F}_{ij}(\theta)\cdot C_j \tag{5}$$

where $\mathcal{F}_{ij}(\theta)$ is a $3M \times 3M$ Hermitian matrix periodic in θ, given by

$$\sum_p F_{ij}^{p}\cdot \exp(ip\theta) = \mathcal{F}_{ij}(\theta) \tag{6}$$

with the notation $n' - n = p$.

Solving the system of Eq. 6, we get $3M$ positive values for w_λ^2 for each value of θ and $3M$ eigenvectors, C_j. The $3M$ $w_\lambda^2(\theta)$ functions are periodic in θ with a period 2π. The functions $f = w(\theta)$ are called the dispersion relations (Califano, 1976). θ can take values between $[-\pi, \pi]$. $w(\theta) = w(-\theta)$ because of time reversal invariance. Because $\mathcal{F}_{ij}(\theta)$ is a Hermitian matrix, its eigenvalues will be real and its eigenvectors real and orthonormal.

The solutions of Eq. 6 are called the normal modes of vibration of the molecule. Each normal mode, convention-

ally represented as a standing wave, may be seen as waves traveling in opposite directions. $\theta > 0$ corresponds to waves traveling in the positive direction of the helix axis and $\theta < 0$ to waves traveling in the negative direction. Like the three-dimensional normal modes of crystals, the quanta of the macromolecular vibrational field are referred to as phonons.

The triple helix, as considered in the present investigation, is an infinite polymer, and its vibrational spectrum has $3M$ branches (M is the number of atoms in the unit cell). Four of these vibrational modes are zero frequency acoustic modes. Two of these branches have ω_λ approaching 0 as $\theta \rightarrow 0$, corresponding to longitudinal sound wave mode and a torsional mode. There are two other zeroes at $\theta = 30°$ and $\theta = -30°$, and they represent circularly polarized waves with displacements in the plane transverse to the axis of the helix. The linear combination of the two circular waves (which are degenerate and any combination of which is also a normal mode) form the two transverse acoustic modes. For $\theta = \pm 30°$, where $w = 0$, they become the two center-of-mass displacements perpendicular to the helix axis. The branches that do not reach $w = 0$ at any point are called the optical branches. The optical modes are characterized by the absence of center-of-mass motion of a unit cell during the wave propagation. Because the triple helix is a big molecule, it has very low lying optical modes.

The force constants

When the force constant matrix for the triple helix was constructed, the main assumption was that the strength of a bond between a certain pair of individual atoms is the same in the triple helix and the double helix.

Van Zandt et al. (1977) refined the backbone force constants for the double helix, and Takahashi et al. (1973) refined the force constants for the bases, starting with an initial set of values from the literature for similar atoms in similar bonding configurations in smaller molecules.

The force constants arising from the valence force field are the stretch force constants, angle bend force constants, and torsion force constants. The stretch force constants are the force constants that determine the force along the chemical bond between two atoms, stretching or compressing it. The angle bend force constants involve the existence of two valence bonds starting at the same atom. The angle between the two bonds will have an equilibrium value due to quantum orbital effects. When the displacement of the atoms modifies the equilibrium value of the angle, the angle bend force will act to restore it to the initial value. The torsional force constants can be defined when four atoms are connected through three consecutive bonds. The torsion interaction opposes a rotation of the two lateral bonds about the middle bond from their equilibrium positions.

Besides the valence force constants in triplex DNA, there are the hydrogen-type bonds. They are weaker than the valence bonds and have little influence on the high-frequency vibrational modes. This is why it is very difficult to refine them from experimental data. The DNA spectra in the lower frequency region are so crowded that it makes it impossible to assign any particular modes to a certain type of bond or motion of the molecule. (A theoretical approach to this problem has been designed, but the experiment that would confirm its validity has not been carried out yet (Dadarlat, 1994). The hydrogen bonds have been studied in simple systems, and empirical formulas have been found that give the H-bond force constants as a function of the donor-acceptor pair involved and the distance between the end atoms (Schroeder and Lippincott, 1957). We used the Lippincott-Schroeder potential function (Schroeder and Lippincott, 1957) to get the hydrogen bond force constants for the A and B conformations of triple-helical DNA. The hydrogen bond lengths and the corresponding force constants for the two conformations are listed in Table 1.

The chemical interactions described by the valence forces and the H-bond forces are short-range interactions. Besides the short-range interactions, there are the long-range interactions. Even though they are weaker in magnitude, they play an important role in the stability of the macromolecule. From this category we took the van der Waals and electrostatic interactions into consideration.

The electrostatic interactions arise between the atoms that have an unbalanced charge. The phosphate groups have a large uncompensated negative charge. This charge induces a small unbalanced charge on almost all of the atoms in the macromolecule by charge transfer. The effective charges on each DNA atom have been calculated for the double helix by Miller (1979). We assumed that the atoms in the triple helix have the same effective individual charges. All of the force constants were calculated at room temperature (293 K).

THE STABILITY OF A- AND B-FORM TRIPLE-HELICAL DNA IN THE PRESENCE OF COUNTERIONS

Counterions in triplex DNA solutions

The triple DNA polymer is a negatively charged macromolecule with approximately three units of negative charge on each unit cell (carried mainly by the phosphate groups). This charged helical polymer is immersed in an ionic aqueous solution. The near neighborhood of the macromolecule contains positively charged metallic counterions. (The counterions could be monovalent (Li^+, Na^+) or divalent (Mg^{2+}, Ca^{2+}, Zn^{2+}).) The surrounding water and counterions play a very important role in stabilizing the equilibrium configuration of the triple-helix DNA. The interactions of the charged counterions with the partial atomic charges on the polymer atoms are mainly electrostatic in nature and influence the dynamics of the system in general and the normal modes in detail. The counterions play important roles in the structural transitions and aggregation of DNA. It has been shown that the concentration, charge, and size of

the counterions (Cheng and Pettitt, 1992) strongly influence the dissolved DNA polymer.

When the normal modes of vibration for the triple-helix DNA polymer are calculated, the complete system considered is composed of a long cylinder containing the triple DNA molecule, with the radius of the molecule (12 Å for the B conformation and 10 Å for the A conformation) and a cylindrical shell with a width of 3.1 Å (the width of one water molecule) filled with water molecules and counterions and the bulk water (Fig. 1). The cylindrical shell that surrounds the triple DNA molecule is called the hydration sheath. To study the influence of the long-range nonbonded forces and the surrounding layer of water on the dynamics of triple DNA, we used the effective field approach developed by Saxena and Van Zandt (Saxena et al., 1989) for the double helix.

In this approach, an explicit dynamical coordinate is introduced to account for the motion of the hydration sheath. The water sheath-polymer combination is neutral because of the positive charges of the counterions present in the hydration sheath. We considered the case in which the counterions that neutralize the total charge of the triplex DNA are three Na^+ ions for each base triplet in the polymer. The type of triple helix we are working with requires monovalent Na^+ to be rendered stable. Other types of triplexes become stable only when divalent ions are present (Mg^{2+}). Another essential feature of this approach is that the nonbonded long-range forces, electrodynamic in nature, are expressed in terms of local electric fields. The local electric fields are determined using Maxwell's equations with appropriate boundary conditions that reflect the geometry of the system (one set of conditions for the polymer-water sheath interface, and another one for the water sheath-bulk water interface). These fields are then coupled to the local partial atomic charges of the atoms within the unit cell of the polymer and the counterions in the hydration sheath. The effect of this field on the aqueous medium is included by means of a measured frequency-dependent dielectric constant.

The three charged counterions interact with the macromolecule through direct Coulomb interactions with the partial atomic charges and through van der Waals-type forces with all of the other atoms in the unit cell. This leads to equilibrium positions of the counterions near the vicinity of the macromolecule. For the case of the double helix, Manning (1978) has suggested that the counterions in an aqueous polyelectrolyte solution surrounding a charged polymer can be confined near the polymer in two different ways. When the counterions are in direct contact with one or more charged groups on the polymer, they are considered to be site bound, fixed to certain positions in the hydration sheath. In the other situation, the counterions are forced to remain close to the macromolecule, but are free to move on its surface, and they are considered to be area bound or territorially bound. The area-bound counterions will be attracted to the polymer as a whole by the negative charges residing there but, once close to the polymer surface, will be free to wander around, encountering small perturbations in their random trajectories.

However, in the real situations, with DNA having different relative humidities (RHs), it is quite possible that between the two extremes we encounter partial or temporary site binding. Here we take the position that the counterions spend time in the local minima of the potential surfaces when their energies are low, and then, under statistical fluctuation, become excited and escape from the potential well, wander about for a while, and then fall back into another potential well.

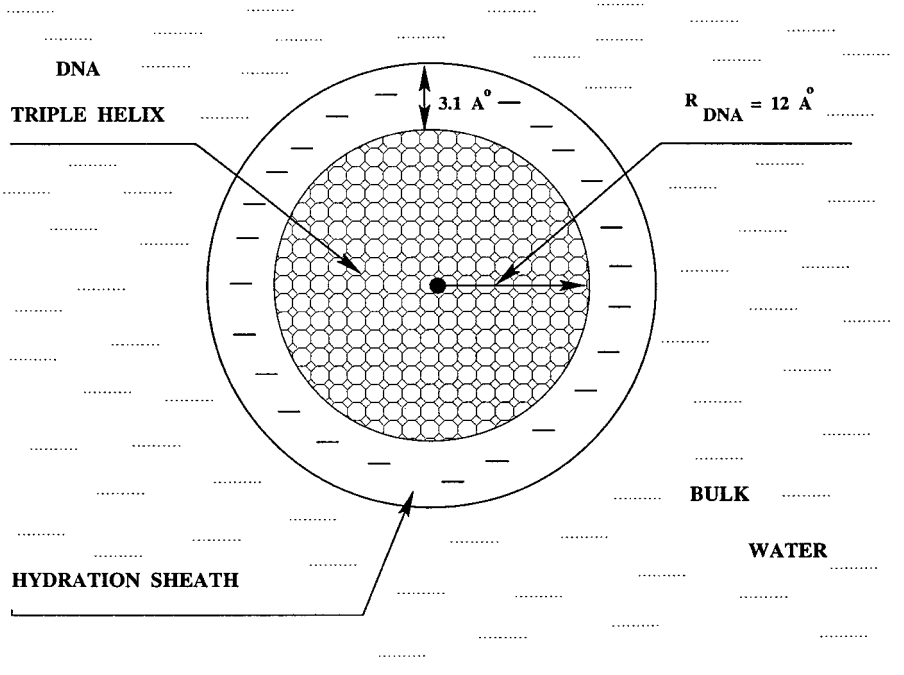

FIGURE 1 The triplex DNA − hydration sheath + counterions − bulk water system.

To characterize this situation a continuous parameter, X_c, has been introduced. X_c can take any value in the [0, 1] interval. $X_c = 0$ corresponds to the case in which the counterions are area bound. $X_c = 1$ would correspond to the site-bound case. Any value in between describes a certain degree of boundedness.

For the case of site-bound counterions, we have to introduce explicit dynamical coordinates for the motion of each counterion, besides the dynamical coordinate describing the motion of the hydration sheath. In the case of area-bound counterions, the mass and charge of the counterions are distributed over the cylindrical sheath volume.

For the triple-helical DNA, with 61 atoms in the unit cell, there are 183 degrees of freedom. To these we have to add 9 degrees of freedom, corresponding to the three counterions assigned to the unit cell, and the one degree of freedom allowed to the hydration sheath. The complete system has 193 degrees of freedom.

Equations of motion for the triplex DNA with counterions and the hydration sheath

Assuming the partial site binding condition as a most general case, we assign mass-weighted dynamical coordinates $\bar{\xi}_l^\alpha = \sqrt{X_c M_c}\ \xi_l^\alpha$ to the motion of the three counterions within a unit cell. $\alpha = x, y, z$; $l = 1, 2, 3$; and M_c is the mass of a counterion. $X_c M_c$ is the average coupled site-bound mass loading to the polymer; we are going to call it the effective mass of the counterion. ξ_l^α is the α component of the displacement vector ξ_l of counterion l.

The kinetic energy associated with the counterion motion will be an "effective kinetic energy" and can be written as

$$K_c^{\text{eff}} = \frac{1}{2} X_c M_c \sum_{l,\alpha} (\dot{\xi}_l^\alpha)^2 \tag{7}$$

The variables in this equation have the same significance as in the previous paragraph. $(1 - X_c) * M_c$ of the total mass of the counterions is spread in the water sheath, and it follows its motion (the linear density of the water sheath will be a function of X_c, too). The potential energy associated with the counterions can be expressed as

$$P_c^{\text{eff}} = \frac{1}{2} X_c \sum_{ij} F_{ij}\, q_i\, q_j \tag{8}$$

If one of the dynamical coordinates is representing the counterion motion, the force constant that comes into the potential energy calculation will be scaled by $\sqrt{X_c}$.

Assuming only longitudinal motion of the water sheath, we represent this motion by a dynamical variable $\bar{s} = \sqrt{h\rho}s$, where s represents the displacement amplitude of the near water sheath containing the counterions. $\rho = \rho_0 + 3(1 - X_c)M_c/h$ is the linear mass density of the sheath, where ρ_0 is the linear mass density of water, M is the counterion mass, and h is the helix rise per unit cell. The effective field approach applied to triple-helix DNA (Saxena and Van Zandt, 1992), with an explicit dynamical coordinate for the motion of the hydration sheath and three dynamical coordinates for each counterion, yields the following equations of motion for the triple-helix system:

$$-\omega^2 q_i^\alpha = \sum_{j,\beta} D_{ij}^{\alpha\beta} q_j^\beta + \acute{e}_i E_\alpha - i\omega\Gamma_i(\bar{s} - q_i^\alpha \eta_i)\delta_{iP}\delta_{\alpha z} + \sqrt{X_c} \sum_{l,\beta} F_{il}^{\alpha\beta} \bar{\xi}_l^\beta \tag{9}$$

$$-\omega^2 \bar{\xi}_l^\beta = \sqrt{X_c}[\acute{e}_c E_\beta - i\omega\Gamma(\bar{s} - \bar{\xi}_l^\beta \mu_c)\delta_{\beta z} + \sum_{j,\alpha} F_{lj}^{\beta\alpha} q_j^\alpha] + X_c \sum_{l'\alpha} C_{ll'}^{\beta\alpha} \bar{\xi}_{l'}^\alpha \tag{10}$$

and

$$-\omega^2 \bar{s} = -k^2 v_w^2 \bar{s} - \acute{\lambda} E_z - i\omega \sum_i \Gamma_i(q_i^z - \bar{s}/\eta_i)\delta_{iP} - i\acute{\gamma}\omega\bar{s} - i\omega\Gamma\sqrt{X_c}\sum_l (\bar{\xi}_l^z - \bar{s}/\mu_c) \tag{11}$$

where ω is the frequency of a mode of the system. $q_i^\alpha (\alpha = x, y, z)$ are the components of the mass-weighted displacement amplitude vector $\mathbf{q}_i$ of atom i, defined by $\mathbf{q}_i = \sqrt{m_i}\ \delta\mathbf{r}_i$, with mass m_i and the corresponding coordinate $\mathbf{r}_i$ of a monomer.

Equation 9 describes the motion of the atoms in the triplex DNA, Eq. 10 describes the motion of the partially bound counterions, and Eq. 11 describes the motion of the water sheath. The first term on the right side of Eq. 9 contains the contributions to the dynamical matrix, within the harmonic approximation, from the bonded interactions (bond stretch, angle bend, and torsion) between polymer atoms. This term also contains contributions from the Coulomb and the van der Waals interactions between the pairs of triplex DNA atoms within a unit cell, and contributions from the van der Waals interactions between pairs of triplex DNA atoms within the unit cell and the nearest-neighbor cells on both sides (cell 1 and cell −1). Collection of all of these forces is contained in the force constant matrix $D_{ij}^{\alpha\beta}$.

The third term on the right side of Eq. 9 incorporates the dissipative forces at the polymer-solvent interface, with a similar term in Eq. 11, the equation of motion for the water sheath. Equation 11 also contains the term $-i\omega\acute{\gamma}\bar{s}$ for damping at the sheath–bulk water interface. The first term on the right side of Eq. 11 represents the elastic contribution to the sheath motion. v_w is the sound speed in bulk water, and k is the wave vector for propagation of the disturbance along the triple DNA-solvent system ($\eta_i \equiv \sqrt{h\rho/m_i}$). Kronecker deltas δ_{iP} and $\delta_{\alpha z}$ restrict the frictional forces at the triple DNA-sheath interface to the coupling of the z component of the motion of phosphorus atoms on the three backbones with the longitudinal motion of the sheath. The damping parameter $\acute{\gamma}$, for the sheath-bulk water coupling, is derived from the viscosity of bulk water (Dorfman and Van Zandt,

1984). Some of the parameters used in the triple helix with counterions and water sheath equations of motion are similar to those used for the double helix in earlier calculations (Saxena et al., 1989, 1991; Van Zandt and Saxena, 1989).

The last terms on the right side of Eq. 9 represent the contribution of the counterions to the equation of motion for the atoms in the triplex. The last term in Eq. 10 describes the interactions between the counterions through the $C_{ll'}^{\beta\alpha}$ force constants. The second to last term in this equation contains the elements $F_{lj}^{\beta\alpha}$ of the force constant matrix of direct interactions between counterions and triplex DNA polymer. A similar, equal, and opposite term appears in Eq. 9 for the motion of atoms in the triplex DNA monomer. These are action/reaction pairs. We have introduced a damping term, the second term in Eq. 11, between the z-motion of the counterions and the motion of the water sheath. The constant Γ in this term couples the z-motion of the counterions with the water sheath motion. An elementary calculation based on the DC conductivity of ionic solutions shows that Γ is so large that they move together almost perfectly as if the counterions were glued to the water ($\mu_c = \sqrt{h\rho/M_c}$).

In the above equations, X_c comes in different powers. This calls for some explanation. X_c may be considered either a fractional occupation time of a site binding position as mentioned before, or alternatively for a long polymer, a fraction of linked polymers site occupied at any one time. For calculating the dynamics of collective running waves on the polymer, it is as if every site were occupied by a lighter, less stiffly bound ion. Thus the force constant appearing in Eq. 9 for ion-atom binding needs a factor X_c. In mass-weighted coordinates, all of the force constants are divided by the square roots of masses of the respective atoms. Hence the effective ion force constants are divided by the root effective mass, and thus by $\sqrt{X_c}$ as well as $\sqrt{M_c}$. This is unsatisfactory, because it leaves hidden dependences of X_c in the constants of the equations of motion. Thus instead, we use $F_{il}^{\alpha\beta}$ defined without $\sqrt{X_c}$ in the mass denominator. The overall fractional effectiveness parameter X_c is reduced thereby to $\sqrt{X_c}$, but all X_c dependence is now explicit. Corresponding corrections occur in the terms of Eqs. 10 and 11.

The last term in Eq. 10, the force constant matrix contribution arising from counterion-counterion interaction, contains X_c for the effectiveness parameter, as it involves pairs of counterions. The three counterions in the vicinity of the phosphate groups are far apart, so this term involves relatively smaller contributions. (In the triplex B conformation, the adenine phosphate is 12.22 Å away from the thymine2 phosphorous atom and 20.65 Å from the thymine1 P atom.) For the reasons discussed in an earlier paragraph, this term contains X_c for the effectiveness parameter, as it involves pairs of counterions. When we take the Coulomb interaction between counterions and other atoms in the triplex, an effective charge of $X_c e_c$ enters the force formula. The rest of the charge, $(1 - X_c)e_c$, is uniformly distributed over the water sheath that surrounds the unit cell.

The nonbonded, long-range interactions between distant parts of the polymer and corresponding counterions on distant monomers are accounted for in terms of the effective electric field (Saxena et al., 1989; Saxena and Van Zandt, 1990) **E** with components E_α acting on the partial atomic charges on the polymer atoms and the counterion charges within the sheath. These interactions are represented by the second term on the right side of Eq. 9 and the first right-side term of Eq. 10. The local effective field approach uses the translational symmetry imposed by repeated identical monomers to set up periodic boundary conditions. This means that the electric field will have the same periodicity as that of the chain. Thus for an infinite chain in its surrounding dielectric medium, Maxwell's equations and the related electrodynamic problem can be solved using a cylindrically symmetric coordinate system (Jackson, 1975). The solutions of the Maxwell's equations are propagating periodic fields along the axis of the polymer. These fields are well represented by Bessel functions with infinite boundary conditions. In Eqs. 9 and 10 the local field terms contain the scaled charges $\acute{e}_i = e_i/\sqrt{m_i}$, where e_i is the partial charge on triple DNA atom i within a monomer. $\acute{e}_c = e_c/\sqrt{M_c}$ is the scaled charge on a counterion. $\acute{\lambda} = \lambda/\sqrt{h\rho}$ is the mass-weighted linear charge distribution on the water sheath, and $\lambda = -\Sigma_i\, e_i - 3 * X_c e_c$ is the total average charge of the area-bound part of the counterions within the water sheath. The summation runs over all of the charges in the triplex DNA macromolecule (not including the counterions). As before, we have assumed complete charge neutrality within the molecule-sheath system. Poisson-Boltzmann theory indicates that this assumption is correct to ~95%.

The radial and longitudinal electric fields E_r and E_z are those found by Saxena et al. (1989):

$$E_r(q, r) = E_1(q)H_1^1(\kappa r) \tag{12}$$

and

$$E_z(q, r) = E_0(q)H_0^1(\kappa r) \tag{13}$$

The amplitudes E_1 and E_0 are determined by the boundary condition at the interface between the hydration sheath and the bulk water. H are Hankel functions. κ is given in terms of wave vector q, the frequency ω of an excitation along the polymer chain, the dielectric constant ϵ_{out}, and the DC electrical conductivity σ of the hydration sheath:

$$\kappa = \{-q^2 + \epsilon_{out}\mu_0\omega^2 + i\sigma\mu_0\omega\}^{1/2} \tag{14}$$

Here μ_0 is the constant of magnetostatics. The frequency-dependent dielectric constant of the medium $\epsilon_{out}(\omega)$ is given by (Pethig, 1979)

$$\epsilon_{out}(\omega) = \frac{\epsilon_{dc} - \epsilon_\infty}{1 + i\omega\tau_s + \epsilon_\infty} \tag{15}$$

ϵ_{dc} and ϵ_∞ are the zero-frequency static dielectric constant and infinite frequency dielectric constant of the aqueous medium, respectively. τ_s is the dielectric relaxation time of

the solvent medium. (We use a dielectric relaxation time of 7.9×10^{-12} s found by microwave absorption measurements (Garner et al., 1989).) In Eq. 17, for ϵ_{dc} we have used a value of $41.0\epsilon_0$, corresponding to water with a counterion concentration (Mohan et al., 1993) of ~1 M. ϵ_∞ was taken to be $1.77\epsilon_0$ from the optical index of refraction. We used different dielectric constants for different chemical groups within the unit cell (Yang et al., 1995). When atoms i and j interact and belong to two different groups, the dielectric constant used in the Coulomb force calculation was $\epsilon = \sqrt{\epsilon_i \epsilon_j}$. The dielectric constants for nominated chemical groups in the triple-helical DNA are listed in Table 2. To avoid double counting, no Coulomb interaction has been considered between the atoms belonging to the same chemical group. These interactions have been taken care of when the force constants have been calculated.

The positions of the counterions for the partial site-bound case

One important and difficult step in adding the counterions to the triple DNA–hydration sheath system is to determine their equilibrium, site-bound positions relative to the set of coordinates used for the triplex DNA. There have been a number of papers involving this question about the DNA double helix. Molecular dynamic simulations of double DNA with counterions (Osman et al., 1991) placed counterions at positions bifurcating the O-P-O angle at a distance of 5.0 Å from the phosphorous. The model used by Lavalle et al. (1991) does not use the position coordinates for the counterions. Young et al. (1989) placed the sodium ions a distance of 2.7 Å radially outward from the free phosphate oxygens, matching it to calculations by Clementi and Corongiu (1981). In this scheme the counterions are ~11.9 Å away from the axis of the double helix, within the water of the hydration sheath.

To include the counterions explicitly in the effective field approach for the triplex, we have to determine the type of interactions between the counterions and the triple DNA polymer atoms that we are going to consider. These interactions are responsible for the counterion binding. The interactions to be included (in descending order of magnitude) are

1. Coulomb interactions between counterions and partial atomic charges on the DNA atoms. Coulomb interactions of the counterions with all of the atoms in the central monomer (cell 0) and in the nearest-neighbor monomers on either side of the central cell were included.
2. Van der Waals interactions between counterions and all of the atoms in the central and in the nearest-neighbor cells. The contributions to the dynamical force constant matrix coming from all of these interactions are included in terms $F_{jl}^{\alpha\beta}$ in Eqs. 9 and 10.
3. The long-range electrostatic interactions of the counterions with the atoms in distant monomers on the chain are accounted for, as for the polymer itself, within the effective field **E.**
4. Counterions may also undergo weak covalent type binding with some of the DNA atoms. For example, depending on the size of the ion core, the outermost s-electron shell of a counterion may hybridize with the s-p electron shells of the free phosphate oxygens, thus giving rise to a weak covalent bonding, because the equilibrium distance of the counterions from these oxygens, as found from our analysis, is ~3.0 Å. Molecular dynamics simulations (Mohan et al., 1993) for triplex DNA concluded that the counterions displayed a very strong equilibrium preference for some direct coordination to the free phosphate oxygens.

This weak covalency is similar to what occurs between proton electron states and s-p shells of acceptor atoms in forming an H-bond. The counterions, having a hydrogen-like outer state structure, may give rise to a very weak hydrogen-bond-like coupling with the free oxygens. In the calculations presented here, we have emphasized the nonbonded forces for most of our analysis. However, because ion species-dependent spectral shifts have been reported, and because these covalencies are the only possible interactions available, we have also calculated the spectra including a weak (ranging from 0.1 to 0.2 mdyn/Å) coupling constant to each free oxygen in the phosphate group. These considerations lead to six more (weak) bonds in the triplex DNA molecule. Allowing for the geometry of the linkages, this gives a total of 0.2–0.4 mdyn/Å bond strength for each counterion. This matches reasonably well the direct coupling free force constant of 0.35 mdyn/Å used by Lavalle et al. (1991) for the counterions' weak bonding in the double helix.

One of the important properties associated with the stability, conformation, and function of any nucleic acid is the spatially varying dielectric response, both within and immediately outside the DNA. The dielectric response significantly influences the strength of the electrostatic interactions among various parts in complex molecular systems (Yang et al., 1995). All DNA contains modestly polar bases, less polar sugars, and negatively charged phosphates. The salt concentration in triplex DNA solutions is higher than in the douplex case, to compensate for the increase in the charge density of the backbones (due to the third phosphate group that comes with the addition of the third strand). Taken all together, it becomes clear that the behavior of the triplex system will be greatly influenced by the scheme used

TABLE 2 Dielectric constants inside triple-helical DNA

Chemical group	ϵ_{in}
Phosphate	$33.0\ \epsilon_0$
Sugar	$2.0\ \epsilon_0$
Adenine base	$3.4\ \epsilon_0$
Thymine base	$3.4\ \epsilon_0$
Bulk water	$41.0\ \epsilon_0$

for simulating the dielectric medium and the values for the dielectric constants themselves inside and outside the helix.

For the dielectric constants inside the triple DNA molecule, we used the values given by Yang et al. (1995), which reflect the different screening effects particular chemical groups in the macromolecule have on the Coulomb interactions. For the dielectric constant outside the helix, we used a value of $41\epsilon_0$ to simulate a salt concentration of 1 M NaCl in water (compared to $68\epsilon_0$ used by Saxena et al. (1989) for the double-helix system with a lower salt concentration and to the dielectric constant for pure water, $71\epsilon_0$). This value is smaller than for pure water because of the strong restriction imposed on the motion of the water by the DNA macromolecules and the ions. The dielectric constant of the whole DNA triple helix is found to be $16\epsilon_0$ (Yang et al., 1995). We considered the following schemes for the distance-dependent dielectric constants:

1. The dielectric constants are those found by Yang et al. (1995) for each chemical group, and no other dielectric constant distance dependence was employed.
2. The dielectric constant is $2\epsilon_0$ up to a distance of 2.0 Å, the average distance to the second near neighbor. For larger distances the dielectric constants will be those of the groups the atoms belong to.
3. The dielectric constant is $2\epsilon_0$ up to a distance of 4.2 Å, the average distance between the centers of mass of two different groups.
4. The dielectric constant is $2\epsilon_0$ up to 2.0 Å and $3\epsilon_0$ between 2.0 Å and 4.2 Å.

The dielectric constants used are listed in Table 2. The particular choice of a dielectric constant of $2\epsilon_0$ for the second near-neighbor interaction is due to the fact that the minimum dielectric constant in the DNA triple helix is $2\epsilon_0$ (it corresponds to the sugar rings). Another parameter we were looking at in this context was the dielectric constant associated with the counterion that becomes site bound in the phosphate group region. We allowed ϵ_{Na^+} to take the values of

- $33\epsilon_0$, the dielectric constant found for the phosphate groups,
- $16\epsilon_0$, the dielectric constant associated with a whole triplex, and
- $41\epsilon_0$, the dielectric constant of the solvent (the solution of NaCl in water).

In evaluating the counterion/triplex DNA contributions to the van der Waals interaction in the dynamical matrix, we have used the same set of van der Waals parameters as those used to describe the interactions in the duplex DNA–water sheath system by Saxena et al. (1989).

We started fitting the position of the counterions in the triplex DNA by placing them opposite the phosphorous atom corner of the rhombus involving the free oxygens and the phosphorous atom in all three phosphate groups. To preserve the local symmetry (the distances between the counterions and the two free oxygens in each phosphate group are kept the same), we allow the counterions to position themselves anywhere along a vector parallel to the direction of the rhombus diagonal that starts at the phosphorous atom. We also allow them to move perpendicular to the O_1-P-O_2 plane (up and down along a perpendicular vector that has its origin on the diagonal of the rhombus, as shown in Fig. 2).

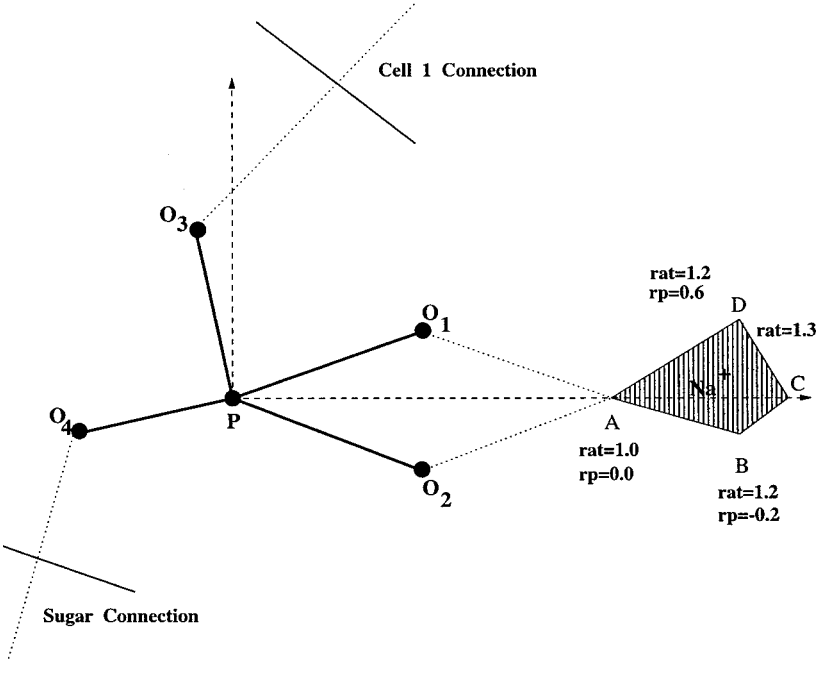

FIGURE 2 Equilibrium domain for the positions of the counterions when $\epsilon^+_{Na} = 16\epsilon_0$.

Stability conditions for the structure with counterions

A normal-mode calculation was performed for each trial position of the counterions, together with the coordinates of the triplex DNA and the interactions between all atoms considered in specified conditions of weak covalent bonding and dielectric constants inside the helix.

In the following paragraphs we are going to use the notation K_c for the weak covalent bonding between the counterions and the free oxygens in the phosphate groups and ϵ_{Na^+} for the dielectric constant associated with the Na^+ counterion. The parameters *rat* and *rp* were introduced to ensure the continuous variation of the positions of the counterions. *rat* lets the counterion slide along the P-Na^+ diagonal of the P-O_1'-Na^+-O_2' rhombus. $rat = 1$ is equivalent to the position of the counterion in the corner of the rhombus 1.71 Å away from the phosphorous atom when $rp = 0$. *rp* is a variable that allows the counterions to move perpendicular to the P-O_1'-Na^+-O_2' plane in steps of 0.1 Å. Any position of the counterion can be precisely determined by knowing the values of *rat* and *rp*.

We are looking for those positions of the counterions (*rat* and *rp* values) and values of K_c and ϵ_{Na^+} that would give us a stable system. This is equivalent to obtaining positive values for all of the eigenvalues of the problem. A 10^{-16} or smaller negative eigenvalue was considered a "hard zero" and consequently was accepted as a good value. Negative eigenvalues ω^2 (bigger than -10^{-16} in our particular case) for the dynamical solution of the vibration problem indicate instabilities, implying an inappropriate choice of equilibrium coordinates and/or the values of ϵ_{Na^+} and K_c. The associated eigenvectors clearly showed that it was the ion positions that were unstable. Thus these positions were modified. We ran repeated calculations of the eigenvalue problem with different possible equilibrium positions for the counterions, different values of the weak covalent bonding between the counterions and the oxygens, and different schemes for the distance-dependent dielectric constants, discarding all trials giving instabilities in the normal-mode spectrum. Final equilibrium positions were found when, with all of the possible interactions included, there were no negative eigenvalues. However, there is no single equilibrium position for the counterions (as previously found for the double helix). We have performed normal-mode calculations on both available structures for triplex DNA, using the structure given by Arnott and co-workers for the A conformation (Arnott and Selsing, 1974) and Raghunathan and co-workers (Raghunathan et al., 1993) for the B conformation. We are going to present here some of the combinations of the parameters described before that rendered the triplex system stable.

Stability conditions for the B conformation triplex DNA

Fixing the counterions in positions close to the phosphate groups, with no covalent bonding between them and the free oxygens, produces an unstable system for all ranges of the counterion dielectric constants and for all distance-dependent dielectric constants inside the triplex.

Using no distance-dependent dielectric constant and with $\epsilon_{Na^+} = 16\epsilon_0$, $K_c = 0.1$ mdyn/Å and $\epsilon_{in} = 2\epsilon_0$ up to a distance of 2.5 Å, the domain of the positions of the counterions for which the triplex is stable is shown in Fig. 2. The extreme positions of the counterions in the corners of the quadrilateral *ABCD* and their distances to the helix axis as well as the distances between the Na^+ and the phosphorous atoms and the distances between the Na^+ and the free oxygens atoms are listed in Table 3. The average Na^+-P distance is 2.03 Å, and the average Na^+-O distance is 1.71 Å.

For $\epsilon_{Na^+} = 33\epsilon_0$, $K_c = 0.1$ mdyn/Å, and $\epsilon_{in} = 2\epsilon_0$ up to a distance of 2.5 Å between the charges, the domain of the positions of the counterions that render a stable DNA triplex system is the area of the triangle *MNR* in Fig. 3. The positions of the counterions and the corresponding distances to the phosphorous and oxygens atoms are listed in Table 4. The extreme point *M* in the *MNR* triangle comes very close to the phosphorous atom (and the oxygens, too). It is very likely that weak covalent bonding between the counterions and the phosphate oxygens is actually a function of distance. Thus for smaller distances between the participating atoms, the covalent bonding is stronger (bigger than the 0.1 mdyn/Å we assumed it to be in this case). Eliminating this point and considering that the system becomes stable when the counterions are in the corner opposite the phosphorous atom of the P-O_1-O_2-Na^+ rhombus, the average distance Na^+-P is 2.1 Å, and the average distance Na^+-O becomes 1.77 Å.

Another set of parameters considered was $\epsilon_{Na^+} = 33\epsilon_0$, $K_c = 0.15$ mdyn/Å, $\epsilon_{in} = 2\epsilon_0$ up to a distance of 2.5 Å between the charges and $\epsilon_{in} = 3\epsilon_0$ between 2.5 Å and 4.2 Å. The specified distances have the meanings described in the previous section. For this set of parameters, the area of stability for the positions of the counterions is much smaller (triangle M' N' R') in Fig. 4. The positions of the counterions and their positions relative to the phosphorous and oxygen atoms are listed in Table 5.

If K_c is bigger, the stability domain increases, too. For $K_c = 0.2$ mdyn/Å and other conditions being the same, the system is stable up to a distance of 2.28 Å between the counterions and the phosphorous atoms. With no explicit dielectric constant dependence on distance inside the helix, and using the dielectric constants given in Table 2, the system is stable, with $\epsilon_{Na^+} = 16\epsilon_0$ and $K_c = 0.15$ mdyn/Å for distances between the phosphorous atoms and the coun-

TABLE 3 Counterion positions in the corners of the *ABCD* quadrilateral

Point	*rat*	*rp*	$d_{Na^+\text{-P}}$ (Å)	$d_{Na^+\text{-O}}$ (Å)	R_{Na^+} (Å)
A	1.0	0.0	1.71	1.48	11.85
B	1.2	−0.2	2.06	1.71	12.12
C	1.3	0.0	2.22	1.83	12.21
D	1.2	0.6	2.14	1.80	12.005

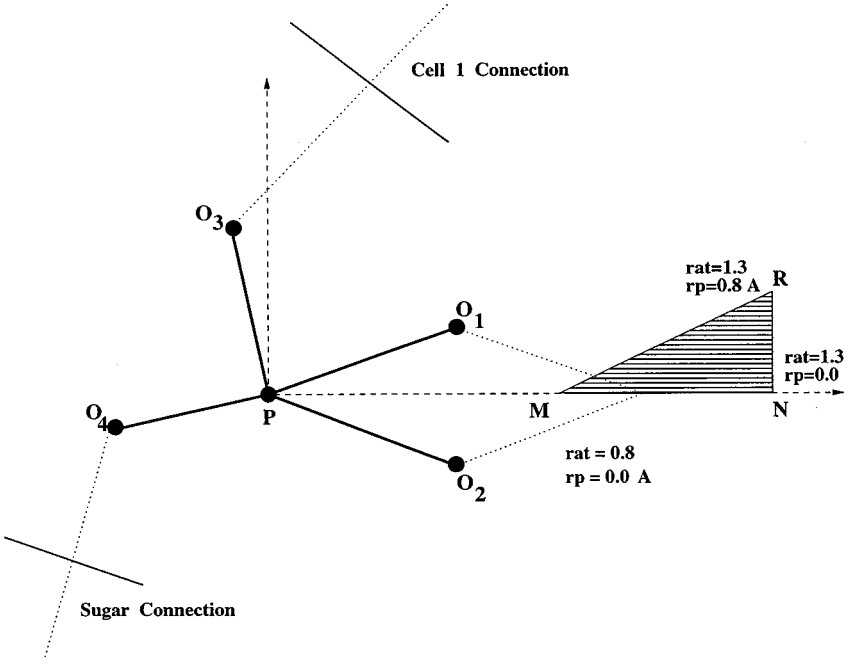

FIGURE 3 Equilibrium domain for the positions of the counterions when $\epsilon^{+}_{Na} = 33\epsilon_0$.

terions stretching from 1.7 Å up to 2.74 Å. The distance between the Na^+ atom and the oxygen atoms varies between 1.48 and 2.2 Å. Using a dielectric constant of $2\epsilon_0$ for the counterion and $K_c = 0.15$, the system is stable for $rat = 1.4$ and $rp = 0.4$, which corresponds to a distance of 2.73 Å between the counterions and the phosphorous atoms and 2.18 Å to the free oxygens in the phosphate groups.

Moving the assumed counterion equilibria in any direction from these equilibrium domains causes instabilities in the form of negative eigenvalues. The eigenvectors associated with the negative eigenvalues indicate free movements of the counterions toward the equilibrium domains.

Choosing among all of the possibilities for the positions of the counterions and the values of the weak covalent bonds proves to be an almost impossible task. The only way we could do that is to calculate the vibrational free energy of the system for all of the simulations considered and choose the lowest one for the solution to our problem.

The B structure is stable for the two extreme cases of area-bound counterions and site-bound counterions, as well as any intermediate cases ($0 < X_c < 1$).

Stability conditions for the A conformation triplex DNA

Using the same parameters and the same kind of interactions for the A structure, our calculations show that this structure is unstable for $X_c = 0$, the area-bound case. A negative eigenvalue of 10^{-4} is obtained when the eigenvalues of the system are calculated. Analyzing the eigenvectors associated with this negative eigenvalue, we find that the A structure tends to modify itself, rotating the adenine and thymine1 strands toward positions closer to the B conformation structure. This tendency is illustrated in Fig. 5. To confirm this assertion we modified the positions of the atoms in the A conformation by adding to them the relative displacement of each atom as indicated by the eigenvector's components. Running the calculations again with these new positions for the atoms, the negative eigenvalue disappears and the system is stable.

All of these results together came as an argument in favor of Raghunatan's work (Raghunathan et al., 1993), which stated that the A structure is stereochemically invalid, with its C_3'-*endo* sugars and its longer hydrogen bonds. The force constants for the hydrogen bonds in the A conformation, calculated following the procedure outlined by Lippincott and Schroeder (1957), are much smaller than similar ones in the B conformation (Table 1).

However, when we add the site-bound counterions in proper positions, we can stabilize the A structure, and we no longer get negative eigenvalues. Because the A conformation is found in samples with lower relative humidities, and because lower relative humidities are more likely to allow site-bound counterions as implied by Manning (1979), the instability of the A conformation in the area-bound case does not come as a big surprise. The positions of the counterions that stabilize the A conformation are listed in Table 6. The distance between the phosphorous atom P and the Na^+ counterion is shorter than for the B conformation case, $d_{Na^+\text{-}P} = 1.88$ Å. The free oxygens of the phosphate groups are 1.59 Å away from the counterions ($\epsilon_{Na^+} = 33\epsilon_0$

TABLE 4 Counterion positions in the corners of the *MNR* triangle

Point	*rat*	*rp*	$d_{Na^+\text{-}P}$ (Å)	$d_{Na^+\text{-}O}$ (Å)	R_{Na^+} (Å)
M	0.0	0.0	1.37	1.31	11.62
N	1.3	0.0	2.22	1.83	12.21
R	1.3	0.8	2.36	2.00	12.1

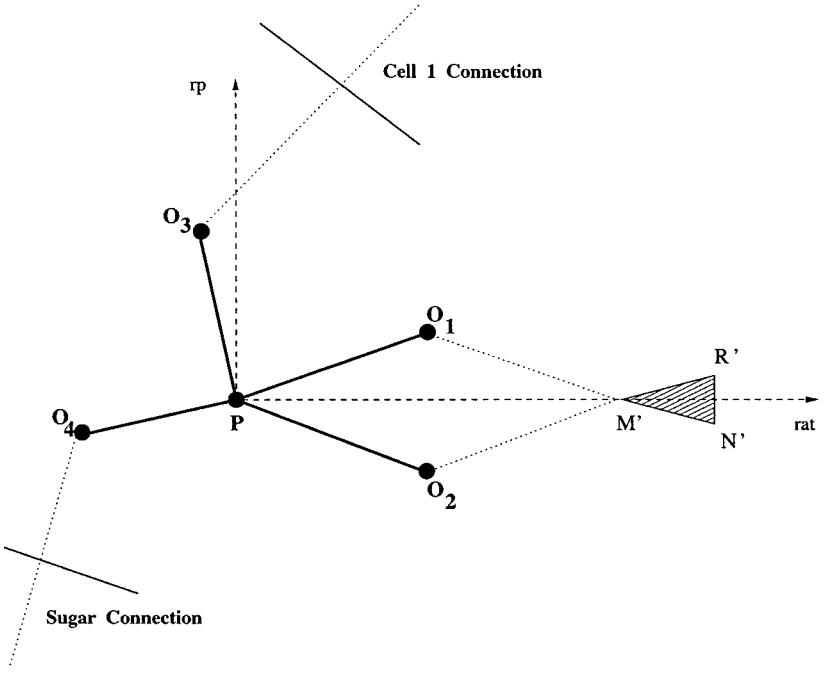

FIGURE 4 Equilibrium domain for the positions of the counterions when $\epsilon_{in} = 2\epsilon_0$ between 2.5 Å and 4.2 Å.

and $K_c = 0.175$ mdyn/Å). The weak covalent bond between the counterions and the oxygens will thus be slightly stronger than in the B conformation case.

Free energy calculations

The free energy F (also called the thermodynamic potential at constant volume) is a function of the state of a thermodynamic system defined as follows (Fermi, 1989):

$$F = U - TS \tag{16}$$

where U is the total internal energy, T is the temperature, and S is the entropy of the system. If the system is in thermal contact with the environment at the temperature T, and if it is dynamically isolated (it is at constant volume and pressure) in such a way that no external work can be performed or absorbed by the system, then the free energy of the system cannot increase during a transformation. A consequence of this fact is that, if the free energy is a minimum, the system is in a state of stable equilibrium.

Our model of the triplex DNA macromolecule allows us to look at it as a system of harmonic oscillators with frequencies given by the normal mode calculation. Having found the normal mode frequencies for the system, calculating the vibrational free energy is theoretically easy. The general expression for F_{vib} (Hill, 1986) in terms of the partition function Q is

$$F_{vib} = -k_B T \ln Q \tag{17}$$

where k_B is Boltzmann's constant and T is the temperature of the system. For each phase difference between oscilla-

TABLE 5 Counterion positions in the corners of the *M′ N′ R′* triangle

Point	*rat*	*rp*	$d_{Na^+\text{-}P}$ (Å)	$d_{Na^+\text{-}O}$ (Å)	R_{Na^+} (Å)
M′	1.0	0.0	1.71	1.48	11.85
N′	1.2	−0.1	2.054	1.705	12.10
R′	1.2	0.1	2.054	1.70	12.07

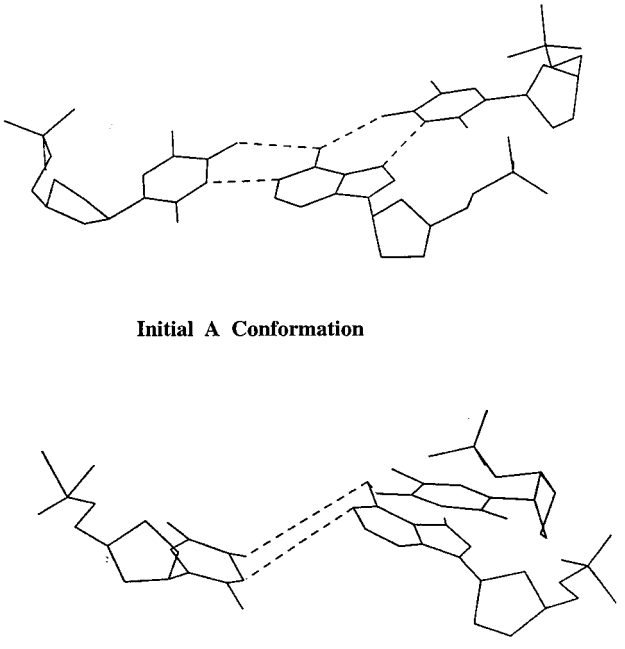

FIGURE 5 Tendency of the atoms in the A conformation to rotate toward better equilibrium positions.

TABLE 6 Counterion positions that stabilize the A conformation

Atom (or ion)	Strand	x (Å)	y (Å)	z (Å)
Ph(atom)		2.883	9.182	−1.705
O(phos)	I	1.618	8.530	−2.112
O(phos)		3.333	10.307	−2.555
Na^+		1.6605	9.8915	−1.2905
Ph(atom)		1.814	−8.757	2.031
O(phos)	II	1.905	−9.865	3.008
O(phos)		0.662	−7.843	2.197
Na^+		0.2225	−9.0480	2.2455
Ph(atom)		−6.757	6.176	−3.130
O(phos)	III	−7.656	6.787	−4.134
O(phos)		−6.533	4.719	−3.265
Na^+		−7.7695	4.9070	−3.1385

tions in adjacent cells, θ, we have $3M$ normal modes of vibration. The total partition function can be written as

$$Q = \prod_{i=1}^{3M} q(\Theta_i). \tag{18}$$

$\Theta_i = h\nu_i/k$ is the characteristic temperature, and q_i is the partition function for a one-dimensional harmonic oscillator and can be written as

$$q_i = \frac{e^{-\Theta_i/2T}}{(1 - e^{\Theta_i/T})} \tag{19}$$

With these, the free energy expression (Prohofsky, 1995) becomes

$$F_{vib} = k_B T \sum_i \ln\left\{2 \sinh \frac{h\omega_i}{4\pi k_B T}\right\} \tag{20}$$

where ω_i is the normal mode frequency. The summation is over all of the states of the system. We calculated the free energy difference between the A and B conformations for different degrees of counterion binding, assuming that the number of occupied energy states, n_i, is the same in the lower frequency region for both conformations. The number of occupied energy states varies with θ as $d\omega/d\theta$, because

$$n_i = \frac{1}{e^{h\omega_i/2\pi k_B T} - 1} \tag{21}$$

The results are constantly showing that the B conformation is energetically favorable to the A conformation. The free energy of the B conformation is lower than the free energy of the A conformation by 1–5 kcal/mol/unit cell. The free energy of the system in the B conformation with the counterions partially site bound ($X_c = 0.5$, $rat = 1.2$, $rp = 0.0$, $K_c = 0.1$) is ~2 kcal/mol/unit cell lower than the free energy of the system with the counterions area bound ($X_c = 0.0$). We could not compare the free energy of the A conformation for the two cases of area-bound and site-bound counterions, because this conformation is not stable for $X_c = 0.0$. Nevertheless, we can certainly say that the A conformation with counterions is more stable (has a lower free energy), because only after the counterion addition in site-bound positions do we get positive values for all of the eigenvalues of the system.

Discussion

Molecular dynamics simulations of ions and water around triplex DNA (Mohan et al., 1993) found the Na^+ ions to be 2.3 Å away from the phosphate oxygens. Our results show that the counterions can take positions within a region situated 1.71–2.49 Å away from the phosphorous atoms, 1.48–2.2 Å away from the oxygens, and 11.85–12.21 Å from the helix axis, within the water sheath.

The model provides a better fit for the B conformation, because we have considered dissolved triple DNA polymer in the dilute limit. Because the relative humidity is large at this dilution, our calculations for a B-conformation poly(dT)-poly(dA)-poly(dT) DNA show a stable system for any degree of counterion binding. Free energy calculations presented in the previous section also support the conclusion that the B conformation is more stable than the A conformation. For drier samples, interhelical interactions, which we did not take into account in our model, are expected to play an important role. The absence of these interactions might explain why the A conformation is not stable at $X_c = 0$.

We should also mention here that the experimental x-ray results of Alexeev et al. (1987) show that the Na-poly dA-poly dT salt is a B-type polymer with similar opposite chains. This might also be the case for triple-helical Na-poly dT-poly dA-poly dT-Na salt considered in our calculations, and the A-conformation is simply not viable for these triple helices.

NORMAL-MODE OSCILLATIONS OF TRIPLEX DNA WITH COUNTERIONS

The frequency dependence of the local field terms and the damping terms in the equations of motion described in the previous section make them nonlinear in ω^2 and thus difficult to solve by direct diagonalization. We have calculated the spectra of the A- and B-form homopolymer poly(dT)-poly(dA)-poly(dT) DNA within the model described in the previous section, using an iterative procedure to get self-consistent eigenvalues and corresponding eigenvectors for each of the eigenvalues separately.

The eigenvalues represent the normal-mode frequencies of oscillation. For each eigenvalue we get a corresponding $3M$ component eigenvector (in our particular case, $M = 64$), which contains information about the relative amplitude of motion of individual atoms or groups of atoms. The eigenvectors can also be used to evaluate the dipole moments associated with each vibrational frequency. The total dipole moment of a certain mode is proportional to the intensity of

the lines observed in IR spectroscopy. The advantage of a normal-mode calculation over spectroscopy is that spectroscopy cannot directly measure the components of the eigenvector representing the amplitudes of individual atomic motions.

The first diagonalization of the interaction matrix is performed without any long-range interaction (the term represented by $E_\alpha e_i$ in the equation of motion in the previous section). We obtain a complete set of solutions $\omega_1, \ldots, \omega_{3M}$. For each ω_i we calculate the mean electric field $E_\alpha(\omega)$ and put it into the equation of motion. The interaction matrix is then rediagonalized and a new set of solutions $\omega_1', \ldots, \omega_{3M}'$ is obtained. If the absolute value of the difference $\delta\omega_i$ between the initial frequency ω_i and the new ω_i' value is smaller than 10^{-8}, ω_i is considered a self-consistent solution of the equations of motion, and the procedure is continued for the next normal-mode frequency. If not, the new ω_i' takes on the role of ω_i and the procedure is reiterated. The information obtained from the eigenvectors is then used to identify and assign the spectral lines from Raman, FTIR, and IR measurements.

To accomplish this task, we project the eigenvectors of each normal mode onto standard vectors representing different motions (translation and rotation) of atoms, groups of atoms, or whole subgroups (sugars, phosphates, bases) in the triplex DNA macromolecule. The internal bond motion with the biggest projections onto the standard vectors are identified as the motions associated with the particular normal mode considered at the time.

Comparing the projections of the eigenvectors on the standard vectors for the triplex DNA with the corresponding ones for duplex DNA will give us information about the changes in the duplex part due to the presence of the third strand.

There have been speculations from spectroscopic measurements about the conformation of the triplex structure. Arnott and co-workers (Arnott and Selsing, 1974), employing their fiber diffraction experiments, concluded that the triplex has A conformation with N-type sugars (C_3'-*endo*). Spectroscopic measurements (IR and Raman spectroscopy) reached the conclusion that the real triplexes have a type B conformation and S-type sugars (C_2'-*endo*) (Thomas and Peticolas, 1983; Howard et al., 1992; Liquier et al., 1991). Based on these experimental results, Raghunathan et al. (1993) came up with the B-structure coordinates for the triplex. We calculate the vibrational phonon spectrum for the two available conformations and compare them with the experimentally existing data to validate the conformational speculations and assertions.

To get an insight into this matter, we are looking at the spectral region between 750 and 900 cm^{-1}, where the marker bands for the N-type and S-type sugars are located. We analyze the eigenvectors of the modes with strong C_2'-*endo* or C_3'-*endo* sugar pucker motions and glycosidic torsions by projecting them onto standard vectors constructed for such motions. We are also looking at the twisting modes ($^2T_3$ and $^3T_2$) perpendicular to the sugar plane formed by C_1'-O_4'-C_4' of the C_2'-C_3' bond, as well as the perpendicular motion to this plane of C_2' and C_3' individually. The pseudorotational angle P for the furanose ring pucker in the three rings belonging to the adenosine chain and Watson-Creek and Hoogsteen thymidine chains in both B and A conformation has been calculated as a function of frequency of vibration. The results are compared to the experimental values obtained through NMR spectroscopy by van Wijk and collaborators (van Wijk et al., 1992) for A and B double-helical DNA.

Another important aspect of the triplex dynamics is the relative motion of the end atoms participating in the interstrand hydrogen bonds. The normal modes corresponding to this type of motion are called the hydrogen bonds' breathing or stretching modes. We constructed standard vectors for the individual hydrogen bond stretching motion and projected them onto the eigenvectors of the motion. The region of the spectra relevant for the breathing or stretching modes turns out to be between 0 and 200 cm^{-1}. We analyze the amplitudes of the motion for both Watson-Crick and Hoogsteen hydrogen bonds.

We also analyze the plasmon mode and compare the dominating frequency with the frequency of the plasmon mode in the double helix. The covalent bond stretching modes are in the region over 1500 cm^{-1}. Whole subunit vibrations (vibrations of their center of mass); phosphate groups of adenine, thymine1, and thymine2; the sugars of adenine, thymine1 and 2; and the bases themselves (adenine, thymine1, and thymine2) are analyzed, and normal modes of vibration are associated with each of them.

The calculation of normal-mode frequencies was performed for values of $X_c \in [0, 1]$. Table 7 shows the variation of the first 20 normal modes with X_c ($K_c = 0.1$, $rat = 1.2$, $rp = 0.0$). A shift of the optical normal modes

TABLE 7 Variation of the first 20 normal modes with X_c

$x_c = 0.0$ cm^{-1}	$x_c = 0.2$ cm^{-1}	$x_c = 0.4$ cm^{-1}	$x_c = 0.6$ cm^{-1}	$x_c = 0.8$ cm^{-1}	$x_c = 1.0$ cm^{-1}
2.69	2.69	2.69	2.69	2.69	2.69
3.49	3.34	3.33	3.33	3.34	3.34
5.10	4.75	4.76	4.76	4.76	4.76
8.88	8.33	8.34	8.34	8.35	8.35
9.52	8.99	9.01	9.03	9.03	9.03
10.31	9.52	9.52	9.53	9.53	9.54
12.27	11.43	11.40	11.37	11.34	11.32
15.42	14.46	14.44	14.41	14.39	14.36
16.34	15.60	15.65	15.67	15.69	15.70
19.70	18.72	18.96	19.01	19.03	19.04
22.14	19.81	20.28	21.21	21.31	21.36
31.08	20.86	24.58	26.98	28.74	30.04
42.87	21.12	24.61	27.02	28.85	30.31
46.50	22.90	25.35	27.53	29.28	30.72
50.53	30.62	30.63	30.64	30.68	30.85
59.01	39.05	39.61	39.92	40.18	40.42
63.46	42.32	43.09	43.49	43.80	44.07
67.14	43.86	44.81	45.28	45.60	45.87
73.66	54.33	55.43	55.84	56.06	56.20
74.43	56.54	57.75	58.28	58.57	58.77

toward lower frequencies becomes evident as the counterions take site-bound positions.

The calculated spectra of the triple DNA macromolecule extends from 0 to 1850 cm^{-1}. After matching normal modes with the characteristic motion they represent, it is the task of the theoretician to find out how well the model designed describes the real systems in the specific experimental conditions. We compared our results with the Raman, IR, and FTIR spectra of triplex DNA in solution (Thomas and Peticolas, 1983; Howard et al., 1992; Liquier et al., 1991; Fang et al., 1995).

Hydrogen bond breathing modes

In the 0–200 cm^{-1} region, the most important features of our normal-mode spectra are the strong amplitudes of the hydrogen bond vibration for both A and B conformations. There are no experimental data available in this frequency region yet for the triple helix. (Only Raman spectroscopy can explore this region successfully. IR spectroscopy is obstructed here by the water strong absorption.) We can compare our results in this region with the confirmed experimentally results of Van Zandt, Prohofsky, and their groups for the double helix. The motion of the end atoms of the H-bonds in the double helix is dominated by the base-base breathing modes found theoretically (from normal-mode calculations by Eyster and Prohofsky (1974) and experimentally by Urabe and co-workers (Urabe and Tominaga, 1985) at ~85 cm^{-1}).

The characteristic breathing modes for the Watson-Crick and Hoogsteen H-bonds in the A conformation are spread over a 40 cm^{-1} region between 75 cm^{-1} and 135 cm^{-1}. The modes with the biggest relative amplitudes are at 76, 88, 107, and 120 cm^{-1} for the Watson-Crick H-bonds and at 76, 81, 87, 114, 121, and 134 cm^{-1} for the Hoogsteen H-bonds. The highest relative amplitude belongs to the mode at 107 cm^{-1} for the Watson-Crick bonds and to the mode at 114 cm^{-1} for the Hoogsteen bonds, respectively. The relative amplitude of ~3.2 of the mode at 114 cm^{-1} suggests that the Hoogsteen H-bonds are more likely to break before the Watson-Crick H-bonds. This is in good agreement with the experimental results of Plum et al. (1990), who show that the Hoogsteen bonded pyrimidine strand is thermally separated from the triple helix at ~30°C.

For the B conformation, we have the strongest relative amplitudes for the Watson-Crick H-bonds at 82, 89, and 101 cm^{-1} and at 89 and 101 cm^{-1} for the Hoogsteen H-bonds. Again, the strongest relative amplitude of the Hoogsteen H-bonds is much higher than that of the corresponding one for the Watson-Crick H-bonds (the ratio is ~3.9:2.8). It can be noted that the breathing modes are shifted toward higher frequencies than that for the double helix (85 cm^{-1}) with 22 to 30 cm^{-1} for the A conformation and 4 to 16 cm^{-1} for the B conformation. These facts could be attributed to the higher rigidity of the triple-helix structure as compared to the double-helix structure.

The relative amplitudes of vibration for both Watson-Crick and Hoogsteen hydrogen bonds are shown in Figs. 6 and 7 for the A conformation and Figs. 8 and 9 for the B conformation.

The plasmon mode

The plasmon mode has been defined as the mode corresponding to the opposite direction motion (along the helix axis) of the positive and negative charges in the DNA macromolecule relative to each other. This mode has been identified by Saxena et al. (1991) to be at 25 cm^{-1} for the double helix.

We found the plasmon mode of the triple helix at 34 cm^{-1} for the A conformation and at 30 cm^{-1} for the B conformation. The shift of 9 cm^{-1} for the A conformation and 5 cm^{-1} for the B conformation can be attributed to the higher rigidity and total mass of the triple helix.

Subunit vibrations

The whole subunit vibration of the three phosphate groups, three sugars, two thymines, and one adenine were very strong in the 0–500 cm^{-1} region (the microwave domain). The motions associated with these modes (translation and rotation of the center of mass of the whole subgroup) are very important biologically. These are the motions that are responsible for the intricate mechanisms that govern the very function of the triplex DNA. Up to this date, there are no Raman spectroscopy measurements in this region for the

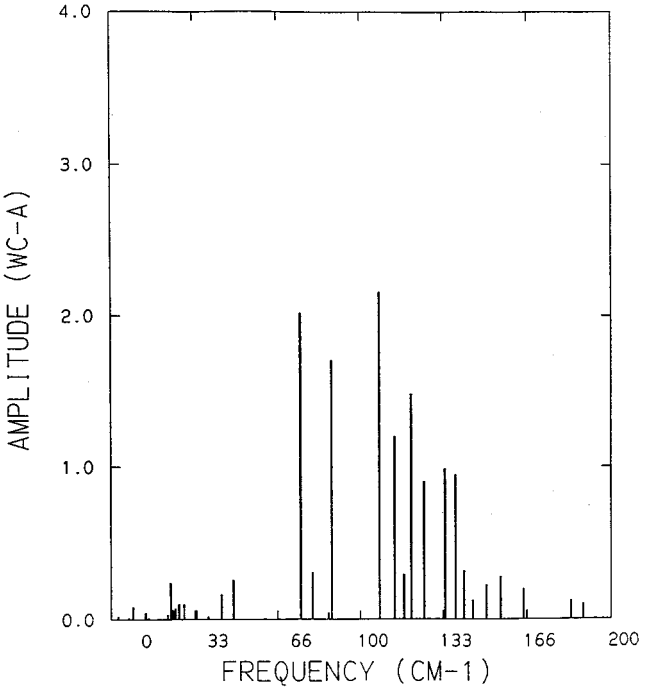

FIGURE 6 Relative amplitude of the Watson-Crick H-bond stretches: A conformation.

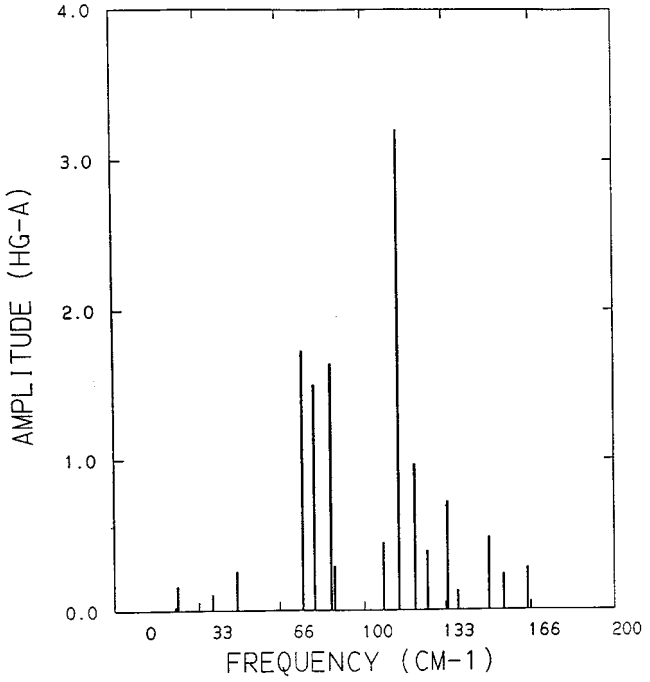

FIGURE 7 Relative amplitude of the Hoogsteen H-bond stretches: A conformation.

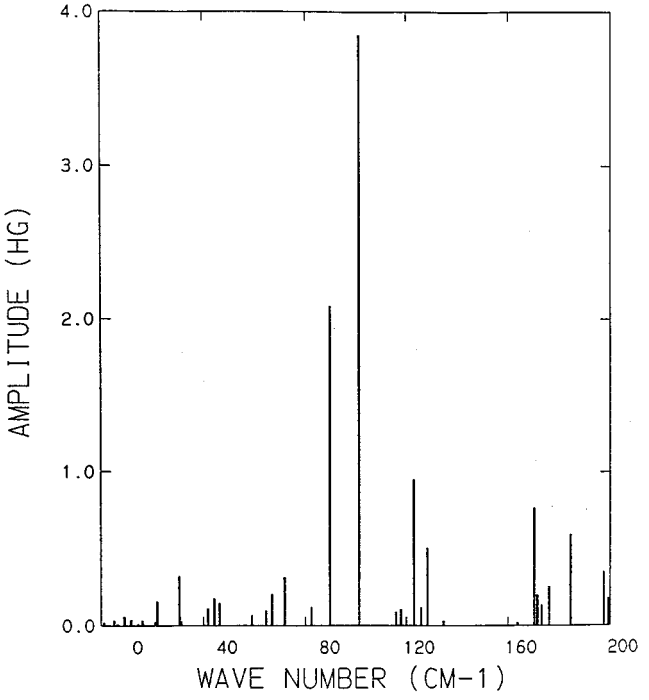

FIGURE 9 Relative amplitude of the Hoogsteen H-bond stretches: B conformation.

triple helix. Even for the double helix, where Raman spectroscopy data exist, the spectra are too crowded and overlapped to discern different modes. With a proper set of experiments (designed by L. L. Van Zandt) and minimization process that has been worked out (Dadarlat et al., 1995), this frequency region should become accessible, and important features of the biological processes involving whole subunit motion could surface.

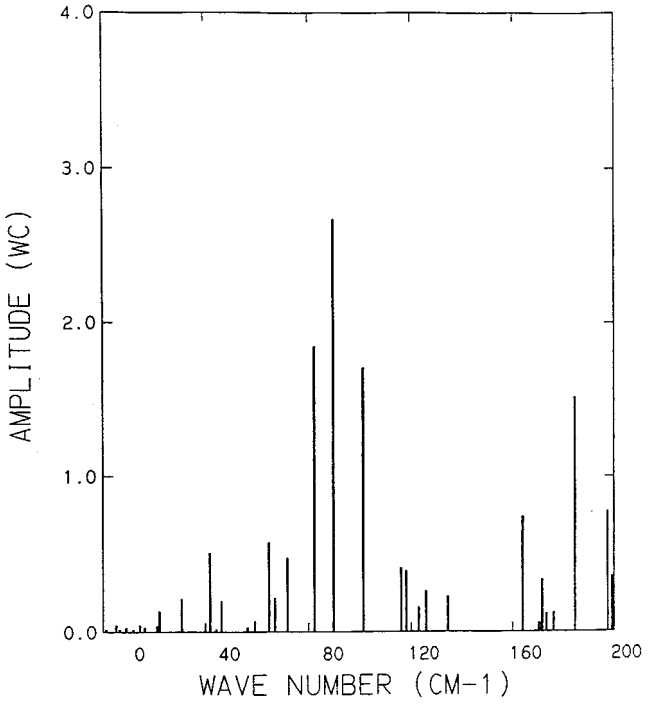

FIGURE 8 Relative amplitude of the Watson-Crick H-bond stretches: B conformation.

The results of our calculations for this frequency region are shown in Table 8. The notation for the nine subunits is as follows:

- Ph(Ad), Su(Ad), and Ad are the adenine phosphate, sugar, and base, respectively.
- Ph(Th1), Su(Th1), and Th1 are the thymine1 phosphate, sugar, and base.
- Ph(Th2), Su(Th2), and Th2 are the thymine2 phosphate, sugar, and base.

Characteristic marker bands for C_2'-*endo* sugars (B conformation) and C_3'-*endo* sugars (A conformation)

It has been shown experimentally that the characteristic marker bands for C_2'-*endo* sugars (specific to the B conformation) are at 830–840 cm^{-1} (Erfurth et al., 1972; Thomas and Peticolas, 1983; Fang et al., 1995; Liquier et al., 1991) and at 810, 862, and 880 cm^{-1} for the C_3'-*endo* sugars in the A conformation, respectively.

We will start our analysis with the B conformation results. Our projections of the eigenvectors on the standard vectors constructed for the stretches of the covalent and double bonds in the plane of the sugar rings in the 600–1000 cm^{-1} show maximum relative amplitudes at 733, 871, 737, 647, and 777 cm^{-1} (in decreasing relative amplitude

TABLE 8 Rotation and translation of the subunits (in the 0–200 cm^{-1} region)

ν (cm^{-1})	Translation (along)	Rotation (about)
3.34	All subunits *z*	Adz
4.76	All subunits *x*, Th1(Ph),Su(Th1),Th2(Ph),Su(Th2)*y*	Not significant
8.35	Ad(Ph), Th1(Ph), Th1x,Ad(Ph),Su(Ad),AdTh2(Ph),Su(Th2)*z*	Th1(Ph),Su(Th1)*y*
8.35	Th2(Ph),Su(Th2)y,Ad(Ph),Th1(Ph),Su(Th1),	Th1*x*
9.02	Th1x, Th2(Ph),Su(Th2)y, Ad(Ph),Su(Ad),Ad,Th1(Ph)	
9.02	Th1,Th2(Ph),Su(Th2)*z*	Ad,Th1(Ph)*y* Th2(Ph)
9.53	Su(Ad),Ad*x* Ad(Ph),Ad*z*	Not significant
19.00	Th1*x*, Ad(Ph),Su(Ad),Th1(Ph),Su(Th1)y Ad,Th1*z*	Th2*y*
25.89	Th1(Ph),Su(Th1)*x* Th1(Ph),Su(Th1)*z*	Not significant
30.64	Ad,Th1,Th2(Ph),Su(Th2)*x* Ad,Th1,Su(Th2)*y*	Th2(Ph),Su(Th2)*z*
40.04	Th1*x* Ad(Ph),Su(Ad),Th1(Ph)*y*	Th1(Ph)*y*
40.04	Su(Th1),Th1*z*	Ad(Ph),Th1
45.57	Su(Ad)*x* Ad(Ph),Ad,Th1*y* Su(Th1)*z*	Ad(Ph),Th1,Th2*y*
56.26	Su(Th1)*x*, *y*, *z*	Th1(Ph),Su(Th1)*y* Th1*z*
61.67	Su(Ad)*x* Su(Ad),Ad,Th1(Ph)*y*	Ad(Ph),Su(Th1)*y* Th1*z*
68.00	Ad,Th1*y*	Su(Th1),Th2*y* Th2
72.36	Ad,Th1 *y*	Ad(Ph),Su(Ad),Ad*y* and Th1*x*
84.50	Ad(Ph),Su(Ad)*x*	Ad(Ph), Ad
111.15	Ad*x* Ad(Ph),Ad*y*	Ad(Ph),Su(Ad),Ad
114.87	Th2(Ph)*x* Th2(Ph)*z*	Th2(Ph)*z*, Th2
124.48	Ad*x* Ad(Ph)*z*	Ad(Ph)*y* Su(Ad),Ad*z*
131.95	Th1(Ph)*x* and *y*	Th1(Ph),Su(Th1)*y* Th1,Th2
135.77	Ad,Th2(Ph)*x* Ad(Ph), Su(Ad),Su(Th2)*y*	Su(Ad)*y* Ad and Su(Th2)*x*
153.75	Ad(Ph)*x* Ad(Ph),Th2(Ph)*y*	Ad(Ph),Su(Ad)*y* Th2*z* and Th2(Ph)
164.57	Th1(Ph),Th1*x* and *y* Th1(Ph),Su(Th1)*z*	Th1(Ph)*y* Su(Th1)*z* Th1
172.23	Su(Th2)*x* Th2(Ph)*y* Th2(Ph),Su(Th2)*z*	Th2(Ph),Su(Th2)
175.47	Ad(Ph),Su(Ad),Ad*x* Ad(Ph)*y* Ad(Ph),Su(Ad)*z*	Ad(Ph), Su(Ad)*z*
189.63	Th1(Ph),Su(Th1),Th1*x* Th1(Ph),Th1*y*	Th1(Ph)*x* Th1*z* Su(Th1)
191.33	Ad*x* Su(Ad),Ad*x*	Ad(Ph)*z* Ad*x* Su(Ad)

order). Covalent bond stretches in the sugar rings are shown in Table 9.

We constructed standard vectors for the twisting vibration of the C_2'-C_3' above and below the C_1'-O_4'-C_4' plane. Again, projecting the corresponding eigenvectors on these standard vectors, we obtain the maximum relative amplitudes at 733, 672, 956, 835, and 830 cm^{-1}. The relative amplitudes of the twisting modes and their characteristic frequencies are listed in Table 10.

We wanted to see what the characteristic frequencies are for the individual vibrations of the C_2' and C_3' atoms perpendicular to the C_1'-O_4'-C_2' plane. The individual vibration of C_2' perpendicular to the plane has its maximum relative amplitudes at 890, 733, 947, 856, 831, and 1017 cm^{-1}. Table 11 shows the main features of the 700–1000 cm^{-1} region from this point of view.

The similar individual vibration of the C_3' atom analysis shows that the maximum amplitudes of vibration are at 693,

TABLE 9 Covalent bond stretches in sugar groups

ν (cm^{-1})	Bond stretch	Sugar group	Relative amplitude
647	C_4'-O_4'	Adenine	0.356
672	C_4'-C_5'	Thymine1	0.258
693	C_4'-C_3'	Thymine2	0.240
733	C_4'-C_5'	Thymine1	0.410
735	C_5'-O_4'	Thymine2-phosphate	0.310
737	C_4'-C_3'	Thymine2	0.390
737	C_5'-O_4'	Thymine2-phosphate	0.270
743	C_5'-O_4'	Adenine-phosphate	0.230
777	C_4'-C_5'	Thymine1	0.320
807	C_1'-C_2'	Adenine	0.251
807	C_5'-O_4'	Adenine	0.240
852	C_1'-C_2'	Adenine	0.200
856	C_1'-C_2'	Thymine1	0.241
863	C_2'-C_3'	Adenine	0.228
871	C_1'-O_4'	Thymine2	0.386
890	C_4'-O_4'	Thymine1	0.241
912	C_1'-O_4'	Adenine	0.245
948	C_4'-C_5'	Thymine1	0.230

TABLE 10 $^2T_3$ twisting modes in sugar groups

ν (cm^{-1})	Sugar group	Relative amplitude
672	Thymine1	0.100
673	Thymine1	0.236
733	Thymine1	0.377
738	Adenine	0.150
738	Thymine2	0.130
777	Thymine1	0.159
831	Thymine1	0.200
835	Adenine	0.210
857	Adenine	0.100
868	Thymine1	0.111
876	Adenine	0.116
876	Thymine2	0.100
956	Thymine2	0.230

TABLE 11 Individual vibrations of C_2' atom perpendicular to the sugar plane

ν (cm^{-1})	Sugar group	Relative amplitude
729	Adenine	0.100
733	Thymine2	0.310
744	Adenine	0.118
831	Thymine2	0.236
855	Adenine	0.218
855	Thymine1	0.230
890	Thymine2	0.370
911	Adenine	0.100
948	Thymine2	0.279
955	Thymine2	0.115
1017	Adenine	0.226
1017	Thymine1	0.158

890, 949, 831, 830, and 857 cm^{-1}. All other frequencies and significant amplitudes of vibration for the C_3' atom are listed in Table 12.

Two bands at 830 and 835 cm^{-1} account for the observed splitting of the 835 cm^{-1} B marker band (Thomas and Peticolas, 1983) in triple-helical DNA. These two bands are associated with the twisting and are perpendicular to the sugar plane vibrations of the C_2' and C_3' in all three sugars. The band at 830 cm^{-1} has major contributions from vibrations in the adenine sugars (relative amplitude 0.277), thymine2 sugars (relative amplitude 0.236), and thymine1 sugars (relative amplitude 0.2). The band at 835 cm^{-1} has major contributions from vibrations in the adenine sugars (relative amplitude 0.21) and thymine2 sugars (relative amplitude 0.212).

The intensity of the band at 835 cm^{-1} is 1.58 times greater than that of the 830 cm^{-1} band, suggesting that the 835 cm^{-1} band is better populated. It should be noted that the band at 835 cm^{-1} does not have any major contributions from the Watson-Crick connected thymine1 sugars.

A careful analysis of the modes corresponding to the maximum relative amplitudes of vibration shows that the experimentally determined marker bands for the C_2'-*endo* sugars come from the twisting modes of the C_2'-C_3' bond, as well as their individual vibrations perpendicular to the sugar plane. This kind of association between the normal mode and the motion that it represents cannot be made experimentally. A normal mode at 808 cm^{-1} that has one-third of the intensity of the 835 cm^{-1} band is proper to the A conformation. Another mode at 856 cm^{-1} is rather close to the 862 cm^{-1} marker band for the C_3'-*endo* sugar type corresponding to the A conformation. This might signify that part of the time the sugars can take on the C_3'-*endo* conformation, a possibility that is not ruled out by the experimental observations of A-T-rich DNA duplexes and triplexes (Thomas and Peticolas, 1983; Fang et al., 1995).

TABLE 12 Individual vibrations of C_3' atom perpendicular to the sugar plane

ν (cm^{-1})	Sugar group	Relative amplitude
693	Thymine2	0.314
743	Thymine1	0.114
777	Adenine	0.116
831	Adenine	0.277
836	Thymine2	0.212
857	Thymine2	0.190
867	Thymine1	0.154
886	Thymine1	0.152
890	Adenine	0.302
947	Adenine	0.132
949	Thymine1	0.259
955	Adenine	0.128
956	Thymine2	0.159
1017	Thymine1	0.160

The same kind of analysis was performed for the A conformation. In the A conformation we have strong bands at 813, 818, and 823 cm^{-1} to account for the observed marker bands for C_3'-*endo* at 813–816 cm^{-1}.

The conclusion of our analysis and the matching between the experimental and calculated frequencies for the sugar marker bands in both A and B conformations are shown in Table 13.

Pseudorotational angle *P*

The pseudorotational angle *P* was calculated using the formalism described in *Principles of Nucleic Acid Structures* (Saenger, 1984). The internal torsional angles for each of the three sugar rings in the unit cell were determined as a function of frequency of oscillation for both B (at $X_c = 0.0$ and $X_c = 0.5$) and A (at $X_c = 0.5$) conformations. Although the average pseudorotational angle is about the same for the three sugars (~183° for the B conformation and 1.1–2.35° for the A conformation), their spread and standard deviation are different from one sugar to another. The addition of the counterions in site-bound positions in the B-form triplex DNA tends to stabilize the motion of the adenosine sugar (the spread of the *P* values goes down from 126.78° to 98°), but gives the thymidine sugars more freedom of motion (the spread of their pseudorotational angles goes up from 101° to 109° for the Watson-Crick strand sugar and from 123° to 138° for the Hoogsteen strand sugar). Our results are summarized in Table 14. Experimental results obtained through

TABLE 13 Characteristic experimental and theoretical modes for sugars in A and B conformation

Conformation	Experimental ω (cm^{-1})	Theory ω (cm^{-1})
B		733
	835	830
		835
		856
	840	871
		890
A	813	813
		818
		823
	862	876
	880	886

TABLE 14 Pseudorotational angle *P* for sugars in A and B conformation

Conformation	Statistics	*P*(Ad) Degrees	*P*(T1) Degrees	*P*(T2) Degrees
B	Mean and std	183.13 (11.42)	182.98 (9.10)	182.73 (9.48)
$X_c = 0.0$	Range	119.44–246.22	143.85–244.82	122.14–245.44
	Spread	126.78	101	123.3
B	Mean and std	182.38 (10.63)	183.6 (10.95)	182.18 (11.91)
$X_c = 0.5$	Range	119.56–217.04	146.96–255.91	106.68–244.57
	Spread	98.0	109	138
A	Mean and std	1.14 (13.7)	1.10 (10.67)	2.35 (8.1)
$X_c = 0.5$	Range	−85.79–73.41	−74.43–38.51	−23.94–68.78
	Spread	159.3	112.84	92.72

NMR spectroscopy by van Wijk and collaborators (van Wijk et al., 1992) for a 20-bp double-helical B conformation showed that the range of the pseudorotational angle values for a 100% S-type conformational purity is 138° to 196° with a mean of 162° for the purine sugar, and 87° to 156° with a mean of 132° for the pyrimidine sugar.

Phosphate and deoxyribose vibrations (1250–1000 cm^{-1} region)

This frequency region contains the characteristic bands for the antisymmetrical and symmetrical phosphate stretch of PO_2^- groups and deoxyribose motion. The experimental data attribute modes at 1024 cm^{-1} to the symmetrical phosphate PO_2^- vibration coupled with the C_5'-O_4 stretch of the covalent bond between the sugar and phosphate groups of the B-type backbone. The mode at 1184 cm^{-1} is characteristic of the A-family DNA and has been assigned to the deoxyribose motion. The antisymmetrical phosphate stretch of PO_2^- groups should be observed at 1204 and 1235 cm^{-1} and reflects the coexistent mixed C_2'-*endo* and C_3'-*endo* geometries of the sugars. The analysis in the next paragraphs is made for the B-conformation theoretical spectra.

Our calculations for this frequency region associate stretches of the P-O_3 bond in the adenine strand with the mode at 1017 cm^{-1}, of the P-O_2 in the thymine1 group with the mode at 1023 cm^{-1}, of the P-O_4 bond in thymine1 with the mode at 1029 cm^{-1}, P-O_2 in thymine1 with the mode at 1097 cm^{-1}, P-O_4 in thymine1 with the mode at 1106 cm^{-1}, and P-O_1 in adenine with the mode at 1260 cm^{-1}. Among the stretches associated with the phosphate group vibrations, the mode at 1097 cm^{-1} has the biggest relative amplitude, and it is close to the characteristic symmetrical vibration of the PO_2^- group, which occurs at 1084 cm^{-1}. This means that our results correctly identify the PO_2^- as belonging to a B-type conformation triple helix.

The characteristic signature of the covalent bond stretching between the sugar and the phosphate groups also appears in our calculations in this region of frequencies. They are located at 1192 cm^{-1} for the covalent bond between sugar and phosphate groups in the adenine strand and at 1238 cm^{-1} for the sugar-phosphate bond in the thymine2 strand. These modes do not quite match with the B-type conformation. Actually, the mode at 1192 cm^{-1} is close to that at 1184 cm^{-1}, which is a characteristic mode for the A-type conformation. Again, we can assume that part of the time, some of the sugars will take on an A conformation for the triplex DNA in aquaeous solution.

Also characteristic for this frequency region are the weak covalent bonding stretches between the counterions and the free oxygens in the phosphate groups: 1114 cm^{-1} for the O_2-Na^+ stretch and 1174 cm^{-1} for the O_1-Na^+ stretch in the thymine2 strand, and 1192 cm^{-1} for the O_1-Na^+ stretch and 1205 cm^{-1} for the O_2-Na^+ stretch in the thymine2 strand. A summary of these considerations is presented in Table 15.

Local base conformation and other features (1250–1700 cm^{-1} region)

The most prominent features of the spectrum in this frequency region are the stretches of the covalent bonds between the backbones (sugars) and the corresponding bases at 1300, 1324, and 1554 cm^{-1}; the deoxyribose vibration in the thymine2 strand at 1326 cm^{-1}; the sugar-phosphate connection stretches at 1386 and 1700 cm^{-1}; the vibrations of the covalent bonds in the adenine base at 1260, 1362, and 1545 cm^{-1}; and the vibrations in the two thymine bases at 1300, 1326, 1513, 1555, 1667, and 1700 cm^{-1}.

Among these modes, the best match with the experimental results is achieved by the 1326 cm^{-1} mode associated

TABLE 15 Stretching modes in PO_2^- groups, between sugar and phosphate groups, counterion signatures

ν (cm^{-1})	Stretch	Relative amplitude
1017	P-O_4 adenine	0.200
1023	Ad(Ph) thymine1	0.228
1023	P-O_4 thymine1	0.270
1097	Th1(Ph) thymine1	0.358
1106	P-O_4 thymine2	0.245
1192	C_5'-O_4 Su(adenine)-Ph(adenine)	0.260
1238	C_5'-O_4 Su(thymine2)-Ph(thymine2)	0.303
1114	O_2-Na^+ thymine2	0.423
1174	O_1-Na^+ thymine2	0.203
1192	O_1-Na^+ thymine1	0.303
1205	O_2-Na^+ thymine1	0.214

with the deoxyribose vibration of the C'_4-C'_5 covalent bond in the sugars of the thymine strands. The frequency experimentally assigned to this vibration is 1328 cm^{-1}.

It has been found experimentally that 1369 cm^{-1} is associated with the coupling between the amino groups and the phosphodiester backbone (the bond between the bases and the sugar-phosphate part of the strands). None of our frequencies corresponding to the same type of motion is very close to it (1300, 1324, and 1554 cm^{-1}). The vibrations of the N_7-C_8-H bond in the adenine group are assigned to the 1344 cm^{-1} mode. Our calculations show that this kind of vibration is at 1260, 1362, and 1545 cm^{-1}.

In the triplex $d(C)_n$-$d(G)_n$-$d(C)_n$, a mode at 1728 cm^{-1} is considered to be the marker band for the presence of the third strand. In our calculations, a mode at 1701 cm^{-1} is correlated with very strong vibrations of the bonds in the thymine2 strand. A strong mode at 1670 cm^{-1} has been associated with the presence of water in the Watson-Hoogsteen groove. We have a very strong similar mode at 1669.32 cm^{-1}, and its dipole moment is among the higher (0.58) dipole moments we obtained for all of the modes. This is a good indication that there is structural water in the mentioned groove.

Bending vibrations of the angles that join the subunits (chemical groups) in triplex DNA

We looked at the maximum relative bendings of the angles that join the subunits in triple-helical DNA (phosphate-sugar, sugar-base) in all three strands. There are 15 specific angles:

- P-$\widehat{O_4}$-C'_5 and C'_4-$\widehat{C'_5}$-O_4 between phosphate and sugar in the adenine strand
- C'_3-$\widehat{C'_4}$-C'_5 in the sugar ring of adenine
- O'_5-$\widehat{C'_1}$-N_9 and C_4-$\widehat{N_9}$-C'_1 between base and sugar in the adenine strand
- P-$\widehat{O_4}$-C'_5 and C'_4-$\widehat{C'_5}$-O_4 between phosphate and sugar in the thymine1 strand
- C'_3-$\widehat{C'_4}$-C'_5 in the sugar ring of thymine1
- O'_5-$\widehat{C'_1}$-N_1 and C_6-$\widehat{N_1}$-C'_1 between base and sugar in the thymine1 strand
- P-$\widehat{O_4}$-C'_5 and C'_4-$\widehat{C'_5}$-O_4 between phosphate and sugar in the thymine2 strand
- C'_3-$\widehat{C'_4}$-C'_5 in the sugar ring of thymine2
- O'_5-$\widehat{C'_1}$-N_1 and C_6-$\widehat{N_1}$-C'_1 between base and sugar in the thymine2 strand

There are no experimental marker bands for this type of motion. Our predicted frequencies for each of these angle bendings are listed in Table 16. Normal-mode calculation for DNA triple helices has been performed by other techniques by Prohofsky and co-workers (Chen et al., 1996, 1997).

TABLE 16 Bending modes in triple-helical DNA

Strand	ν (cm^{-1})	Angle	Relative amplitude
Adenine	887	P-O4-C'_5	0.728
	886	C'_4-$\widehat{C'_5}$-O_4	0.425
	1017	C'_3-$\widehat{C'_4}$-C'_5	0.827
	1174	O'_5-$\widehat{C'_1}$-N_9	0.398
	807	C_4-$\widehat{N_9}$-C'_1	0.716
Thymine1	889	P-$\widehat{O_4}$-C'_5	0.836
	889	C'_4-$\widehat{C'_5}$-O_4	0.784
	1169	C'_3-$\widehat{C'_4}$-C'_5	0.675
	1106	O'_5-$\widehat{C'_1}$-N_1	0.674
	1475	C_6-$\widehat{N_1}$-C'_1	0.822
Thymine2	903	P-$\widehat{O_4}$-C'_5	0.85
	903	C'_4-$\widehat{C'_5}$-O_4	0.873
	1191	C'_3-$\widehat{C'_4}$-C'_5	0.590
	1174	O'_5-$\widehat{C'_1}$-N_1	0.617
	1479	C_6-$\widehat{N_1}$-C'_1	0.881

CONCLUSIONS

We modeled the DNA triple helix ($d(T)_n$-$d(A)_n$-$d(T)_n$) as a very long unidimensional lattice. The macromolecule is surrounded by a hydration layer that has the thickness of one water molecule (3.1 Å). The counterions that balance the negative charge on the polymer are within the hydration sheath and can either float around or be more or less bound to the phosphate groups.

The stability of the triple-helical DNA in both A and B conformations in the presence of counterions has been studied. The stability criteria employed were related to the eigenvalues of the problem. Getting a stable system is equivalent to getting positive values for all of the eigenvalues in specific conditions of counterion binding, weak covalent bonding between the counterions, and the free phosphate oxygens and dielectric constants that correctly reflect the screening inside the macromolecule. In the third section we found equilibrium domains for the positions of the counterions in the vicinity of the phosphate groups. We showed that different specific conditions give different equilibrium domains for the positions of the counterions. For the indicated equilibrium domains (Figs. 2, 3, and 4), the B structure is stable for any degree of binding of the counterions to the atoms in the triple helix. The A conformation is not stable when the counterions are area bound. It becomes stable as soon as the counterions are site-bound in proper positions and make weak covalent bonds with the free oxygens in the phosphate groups. A comparison between molecular dynamics simulation results and our equilibrium positions for the counterions shows that our counterions can be 0.1–0.8 Å closer to the phosphate oxygens. Because we have considered dissolved triple DNA in the dilute limit, our model fits better the B conformation structure and renders it stable for any degree of counterion binding. Adding the counterions in the site-bound positions lowers the optical modes in both conformations.

The information that the eigenvectors associated with each eigenvalue contain is analyzed in the fourth section. Standard vectors associated with particular motions in the macromolecule are projected onto the eigenvectors, and the internal motions with the biggest projections are assigned to the particular normal mode considered. We compared our results with the Raman, IR, and FTIR spectra of triplex DNA in solution produced by Thomas and Peticolas (1983), Howard et al. (1992), Liquier et al. (1991), and Fang et al. (1995).

We showed that the hydrogen bond breathing modes are shifted 4–16 cm^{-1} (for the B conformation) and 22–30 cm^{-1} (for the A conformation) toward higher frequencies as compared with the breathing modes of the double helix (85 cm^{-1}).

The plasmon mode (25 cm^{-1} for the double helix) is also shifted to 30 cm^{-1} for the B conformation and 34 cm^{-1} for the A conformation.

We identified whole subunit vibrations in the microwave domain, 0–500 cm^{-1}. At present there are few experimental data to compare to our results.

The best indication that our model is realistic for the system under consideration came from analyzing the characteristic marker bands for the sugars in both conformations. We were able to match our results reasonably well with the experimentally determined marker bands for C_2'-*endo* and C_3'-*endo* sugars for the B and A conformations, respectively. We showed that strong bands in the 813–823 cm^{-1} region are proper to the A conformation of triple helices. This should answer the question of where the 816 cm^{-1} band in the early work of Thomas and Peticolas (1983) comes from. An interesting aspect of our findings was the fact that both conformations in aqueous solution presented marker bands specific to the other conformation as a minor component of the vibrational spectrum. This leads us to the conclusion that some of the sugars take on both conformations part of the time. We were also able to match some of the phosphate and deoxyribose vibrations and local base conformation features with the corresponding experimentally found marker bands. A mode at 1701 cm^{-1} is associated with very strong vibrations in the thymine2 strand, and we consider it a signature for the presence of the third strand (the corresponding experimental marker band for the $d(C)_n$-$d(G)_n$-$d(C)_n$ triplex is at 1728 cm^{-1}). Free energy calculations for the two conformations show that the B conformation is more stable than the A conformation and adds to the conclusion (Alexeev et al., 1987; Raghunathan et al., 1993) that the A conformation is not proper for triplex DNA in aqueous solution.

This paper is dedicated to the fond memory of Lonnie L. Van Zandt.

This work was partly supported by the Office of Naval Research (ONR), through the Free Electron Laser Center, Vanderbilt University (award no. 12403S9).

REFERENCES

Alexeev, D. G., A. A. Lipanov, and I. Y. Skuratovskii. 1987. The structure of poly(dA)-poly(dT) as revealed by an x-ray fibre diffraction. *J. Biomol. Struct. Dyn.* 4:989–1012.

Arnott, S., and E. Selsing. 1974. Structure for the polynucleotide complexes poly(dA)-poly(dT) and poly(dT)-poly(dA)-poly(dT). *J. Mol. Biol.* 88:509–521.

Benevides, J. M., and G. J. Thomas, Jr. 1983. Characterization of DNA structures by raman spectroscopy: high-salt and low-salt forms of double helical poly(dG-dC) in H_2O and D_2O solutions and application to B, Z and A-DNA. *Nucleic Acids Res.* 11:5747–5751.

Califano, S. 1976. Vibrational States. John Wiley and Sons, New York.

Chan, S. S., K. J. Breslauer, M. E. Hogan, D. J. Kessler, R. H. Austin, J. Ojemann, J. M. Passner, and N. C. Wiles. 1990. Physical studies of DNA premelting equilibria in duplexes with and without homo dA-dT tracts: correlations with DNA bending. *Biochemistry.* 29:6161–6171.

Chen, Y. Z., J. W. Powell, and E. W. Prohofsky. 1997. Vibrational normal modes and dynamical stability of DNA triplex poly(dA)-2poly(dT): S-type structure is more stable and in better agreement with observations in solution. *Biophys. J.* 72:1327–1334.

Chen, Y. Z., E. W. Prohofsky, J. W. Powell, and A. P. White. 1996. DNA-triplex conformation from normal mode and hydrogen bond stability calculations. *Bull. Am. Phys. Soc.* 41:516.

Cheng, Y. K., and B. Montgomery Pettitt. 1992. Stabilities of double and triple-strand helical nucleic acids. *Prog. Biophys. Mol. Biol.* 58: 225–252.

Clementi, E., and G. Corongiu. 1981. IBM DPPG research report POK-1. Technical report, IBM. (New York).

Dadarlat, V. M., V. K. Saxena, and L. L. Van Zandt. 1995. Semiclassical IR/Raman spectroscopy of DNA polymers. *J. Biomol. Struct. Dyn.* 12:a041.

Dorfman, B. H., and L. L. Van Zandt. 1984. Effect of viscous solvent on DNA polymer in fiber. *Biopolymers.* 23:913–926.

Duval-Valentin, G., N. T. Thuong, and C. Helene. 1992. Specific inhibition of transcription by triple helix-forming oligonucleotides. *Proc. Natl. Acad. Sci. USA.* 89:504–513.

Edwards, G., and C. Liu. 1991. Sequence dependence of low-frequency Raman active modes in nucleic acids. *Phys. Rev. A.* 44:2709–2713.

Erfurth, S. C., E. J. Kiser, and W. L. Peticolas. 1972. Determination of the backbone structure of nucleic acids and nucleic acid oligomers by laser Raman scattering. *Proc. Natl. Acad. Sci. USA.* 69:938–941.

Eyster, J. M., and E. W. Prohofsky. 1974. Lattice vibrational modes of poly(rU) and poly(rA). *Biopolymers.* 13:2505–2512.

Fang, Y., C. Bai, Y. Wei, S.-B. Lin, and L.-S. Kan. 1995. Effect of selective cytosine methylation and hydration on the conformation of DNA triple helices containing a TTTT loop structure by FTIR spectroscopy. *J. Biomol. Struct. Dyn.* 13:471–482.

Felsenfeld, A. G., D. Davies, and A. Rich. 1957. Formation of a three-stranded polynucleotide molecule (communication to the editor). *J. Am. Chem. Soc.* 79:2023–2024.

Fermi, E. 1989. Thermodynamics. Dover Publications, New York.

Garner, H. R., A. C. Lewis, and T. Ohkawa. 1989. Measurement of the microwave absorption for small samples in a coaxial line. Preprint.

Hill, T. L. 1986. Statistical Thermodynamics. Dover Publications, New York.

Howard, F. B., H. Todd Miles, K. Liu, J. Frazier, G. Raghunathan, and V. Sasisekharan. 1992. Structure of $d(T)_n \cdot d(A)_n \cdot d(T)_n$: the DNA triple helix has B-form geometry with C2′-endo sugar pucker. *Biochemistry.* 31:10671–10677.

Hsieh, P., and R. D. Camerini-Otero. 1990. Pairing of homologous DNA sequence by protiend: evidence for three stranded DNA. *Genes Dev.* 4:1951–1963.

Jackson, J. D. 1975. Classical Electrodynamics. John Wiley and Sons, New York.

Kim, M. G., V. B. Zhurkin, R. L. Jernigan, and R. D. Camerini-Otero. 1995. Defect-mediated hydrogen-bond instability of poly(dg)-poly(dc). *J. Mol. Biol.* 247:874–889.

Lavalle, N., S. A. Lee, and L. S. Flox. 1991. Lattice-dynamical model of crystalline DNA: intermolecular bonds and the A to B transition. *Phys. Rev.* A43:3126–3130.

Liquier, J., P. Coffinier, M. Firon, and E. Taillandier. 1991. Triple helical polynucleotidic structures: sugar conformations determined by FTIR spectroscopy. *J. Biomol. Struct. Dyn.* 3:437–445.

Macaya, R. F., E. Schultze, P. Sklenar, V., and J. Feigon. 1992. Proton nuclear magnetic resonance assignments and structural characterization of an intramolecular DNA triplex. *J. Mol. Biol.* 225:755–773.

Manning, G. S. 1978. The molecular theory of polyelectrolyte solutions with applications to the electrostatic properties of polynucleotides. *Q. Rev. Biophys.* 11:179–182.

Manning, G. S. 1979. Counterion binding in polyelectrolyte theory. *Acc. Chem. Res.* 12:443–446.

Miller, K. J. 1979. Interaction of molecules with nucleic acids. I. An algorithm to generate nucleic acid structures with application to B-DNA structure and a counterclockwise helix. *Biopolymers.* 18:959–971.

Mohan, V., P. E. Smith, and B. M. Pettitt. 1993. Evidence of a new spine of hydration: solvation of DNA triple helices. *J. Am. Chem. Soc.* 115: 9297–9298.

Moser, H. E., and P. B. Dervan. 1987. Sequence specific cleavage of double helical DNA by triple helix formation. *Science.* 238:645–650.

Nelson, H. C., J. T. Finch, B. F. Luisi, and A. Klug. 1987. The structure of an oligo(dA)-oligo(dT) tract and its biological implications. *Nature.* 330:221–226.

Osman, R., K. Miaskiewicz, and H. Weinstein. 1991. Molecular dynamics simulations of DNA with primary radiation damage. *J. Biomol. Struct. Dyn.* 8:a159.

Pethig, R. 1979. Dielectric and Electronic Properties of Biological Materials. John Wiley and Sons, New York.

Plum, G. E., Y. W. Park, S. F. Singerton, and P. B. Dervan. 1990. *Proc. Natl. Acad. Sci. USA*. 87:9436–9440.

Powell, J. W., G. S. Edwards, L. Genzel, F. Kremer, A. Wittlin, W. Kubasek, and W. Peticolas. 1987. Investigation of far-infrared vibrational modes in polynucleotides. *Phys. Rev. A.* 35:3929–3937.

Prohofsky, E. 1995. Statistical Mechanics and Stability of Macromolecules. Cambridge University Press, New York.

Raghunathan, G., H. Todd Miles, and V. Sasisekharan. 1993. Symmetry and structure of a DNA triple helix: $d(T)_n \cdot d(A)_n \cdot d(T)_n$. *Biochemistry.* 32:455–462.

Saenger, W. 1984. Principles of Nucleic Acid Structures. Springer-Verlag, New York.

Saxena, V. K., B. H. Dorfman, and L. L. Van Zandt. 1991. Identifying and interpreting spectral features of dissolved poly(dA)-poly(dT) DNA polymer in the high microwave range. *Phys. Rev. A.* 43:4510–4517.

Saxena, V. K., and L. L. Van Zandt. 1990. Dynamics of dissolved DNA polymers using frequency dependent dielectric constant. *Phys. Rev. A.* 42:4993–4997.

Saxena, V. K., and L. L. Van Zandt. 1992. Effect of counterions on the spectrum of dissolved DNA polymers. *Phys. Rev.* A45:7610–7621.

Saxena, V. K., L. L. Van Zandt, and W. K. Schroll. 1989. Effective field approach for long-range dissolved DNA polymer dynamics. *Phys. Rev. A.* 39:1474–1482.

Schroeder, R., and E. R. Lippincott. 1957. Potential function model of hydrogen bonds. II. *J. Phys. Chem.* 61:921–924.

Strobel, S. A., and P. B. Dervan. 1991. Single-site enzymatic cleavage of a yeast genomic DNA mediated by triple-helix formation. *Nature.* 350: 172–173.

Strobel, S. A., L. A. D. Stamm, L. Riba, D. E. Housman, and P. B. Dervan. 1991. Site-specific cleavage of human chromosome 4 mediated by triple-helix formation. *Science.* 254:1693–1694.

Takahashi, S., M. Tsuboi, and I. Harada. 1973. Physico-Chemical Properties of Nucleic Acids, Vol. 2. Academic Press, New York.

Thomas, G. A., and W. L. Peticolas. 1983. Fluctuations in nucleic acid conformations. 2. Raman spectroscopic evidence of varying ring pucker in A-T polynucleotides. *J. Am. Chem. Soc.* 105:993–996.

Urabe, H., and H. Tominaga. 1985. Collective vibrational modes in molecular assembly of DNA and its application to biological systems. Low frequency Raman spectroscopy. *J. Chem. Phys.* 82:531.

van Wijk, J., B. D. Huckriede, J. H. Ippel, and C. Altona. 1992. Furanose sugar conformations in DNA from NMR coupling constants. *Methods Enzymol.* 211:286–306.

Van Zandt, L. L., K.-C. Lu, and E. W. Prohofsky. 1977. A new procedure for refining force constants in normal coordinate calculations in large molecules. *Biopolymers.* 16:2481–2487.

Van Zandt, L. L., and V. K. Saxena. 1989. Millimeter-microwave spectrum of DNA: six predictions for spectroscopy. *Phys. Rev. A.* 39:2672–2676.

White, A. P., and J. W. Powell. 1995. Observation of the hydration-dependent conformation of the $(dG)_{20} \cdot (dG)_{20} \cdot (dC)_{20}$ oligonucleotides triplex using FTIR spectroscopy. *Biochemistry.* 34:1137–1142.

Wittlin, A., L. Genzel, F. Kremer, S. Häseler, A. Poglitsch, and A. Rupprecht. 1986. Far-infrared spectroscopy of oriented films of dry and hydrated DNA. *Phys. Rev. A.* 34:493–499.

Yang, L., S. Weerasinghe, P. E. Smith, and B. M. Pettitt. 1995. Dielectric response of triplex DNA in ionic solutions from simulations. *Biophys. J.* 69:1519–1527.

Young, L., V. V. Prabhu, and E. W. Prohofsky. 1989. Calculation of far-infrared absorption in polymer DNA. *Phys. Rev. A.* 39:3173–3179.

Zhurkin, V. B., G. Raghunathan, R. D. Camerini-Otero, and R. L. Jernigan. 1994. A parallel DNA triplex as a model for the intermediate in homologous recombination. *J. Mol. Biol.* 239:181–200.

Ziman, J. J. 1972. Electrons and Phonons. Cambridge University Press, New York.